remote sensing

MDPI

Article

Trends and Lagged Cumulative Associations Between Vegetation NDVI and Extreme Climate Indices in the Yangtze River Basin: A 41-Year Observational Analysis

Xiang Cheng [1], Yaoming Ma [1,2,3,4,5,6,7,*], Xiaohua Dong [1,8], Qiangwei Yu [1] and Chengqi Gong [1]

[1] College of Hydraulic & Environmental Engineering, China Three Gorges University, Yichang 443002, China; chengx@ctgu.edu.cn (X.C.); xhdong@ctgu.edu.cn (X.D.); qwyu@ctgu.edu.cn (Q.Y.); gongcq@ctgu.edu.cn (C.G.)
[2] Land-Atmosphere Interaction and Its Climatic Effects Group, State Key Laboratory of Tibetan Plateau Earth System, Environment and Resources (TPESER), Institute of Tibetan Plateau Research, Chinese Academy of Sciences, Beijing 100101, China
[3] College of Earth and Planetary Sciences, University of Chinese Academy of Sciences, Beijing 100049, China
[4] College of Atmospheric Science, Lanzhou University, Lanzhou 730000, China
[5] National Observation and Research Station for Qomolongma Special Atmospheric Processes and Environmental Changes, Shigatse 858200, China
[6] Kathmandu Center of Research and Education, Chinese Academy of Sciences, Beijing 100101, China
[7] China-Pakistan Joint Research Center on Earth Sciences, Chinese Academy of Sciences, Islamabad 45320, Pakistan
[8] Engineering Research Center for the Ecological Environment of the Three Gorges Reservoir Area, Ministry of Education, Yichang 443002, China
* Correspondence: ymma@itpcas.ac.cn

Highlights

What are the main findings?

- Extreme climate in the Yangtze River Basin shifted toward fewer cold events, more warm events, and intensified heavy precipitation during 1982–2022.
- Vegetation NDVI increased significantly across the basin, with the strongest greening in the middle reaches and clear spatial differences among subregions.

What are the implications of the main findings?

- Warm-related extremes were generally positively associated with vegetation greenness, whereas precipitation extremes showed region-dependent associations, with positive NDVI relationships in the upper reaches and negative relationships in parts of the lower reaches.
- Lagged cumulative responses reveal that antecedent climate conditions and vegetation type should be considered when assessing ecosystem responses to climate extremes.

Check for updates

Academic Editors: Qiang Zhang, Wenlong Song, Xihui Gu and Yadu Pokhrel

Received: 5 June 2026
Revised: 11 July 2026
Accepted: 28 July 2026
Published: 4 August 2026

Copyright: © 2026 by the authors. Licensee MDPI, Basel, Switzerland. This article is an open access article distributed under the terms and conditions of the Creative Commons Attribution (CC BY) license.

Abstract

Extreme climate events can disturb vegetation dynamics and alter ecosystem stability. This study investigated the evolution of extreme climatic conditions and vegetation greenness across the Yangtze River Basin during 1982–2022 by integrating CN05.1 daily meteorological records with the PKU-GIMMS NDVI V1.2 dataset. Using the index framework of the ETCCDI, fifteen extreme weather-related climate indices were calculated. Trend magnitudes were quantified using Sen's slope estimation, while the Mann–Kendall trend test was used to determine the direction and significance of long-term changes. Both standard correlation and lagged cumulative correlation were used to assess NDVI–climate relationships; the latter tested ten predefined windows formed from climate conditions between the current month and three months before each NDVI observation, with the

largest absolute correlation defining the optimal window. The basin experienced a distinct warming signal in temperature extremes during 1982–2022, characterized by reduced occurrences of TN10p and TX10p, together with more frequent TN90p and TX90p events. Precipitation extremes showed an overall intensification, with R95p and R99p increasing by 9.2 mm per decade and 5.6 mm per decade. NDVI also increased throughout the analysis period, with a basin-wide rate of 0.0038 per decade and the fastest greening in the middle reaches at 0.0069 per decade. Vegetation NDVI was generally positively associated with warm-related temperature indices and negatively associated with cold-related indices. The lagged cumulative analysis identified the strongest NDVI–climate associations within windows combining current and antecedent climate conditions, with marked differences among subregions and vegetation types. Because the analyses are correlation-based and did not quantify non-climatic drivers such as land-use change or ecological restoration, the results should be interpreted as statistical associations rather than causal attribution. Overall, these findings characterize how vegetation greenness covaries with extreme climate indices across the Yangtze River Basin.

Keywords: extreme climate indices; NDVI; spatiotemporal variation; lagged cumulative effects; Yangtze River Basin

1. Introduction

Under ongoing global warming, climate extremes have become a major pathway through which climatic variability affects terrestrial ecosystems, as rare events may change in recurrence, severity, persistence, and cumulative magnitude [1]. Extreme heat, cold spells, intense precipitation, and prolonged drought are typical forms of climate extremes, and their abrupt occurrence can generate ecological impacts that persist beyond the event period. These disturbances may alter hydrothermal conditions and plant physiological processes, thereby affecting vegetation growth and terrestrial carbon cycling [2]. The ETCCDI provides an index framework for quantitatively describing temperature and precipitation extremes from several dimensions, including occurrence frequency, intensity, duration, and accumulated amount, which offers a consistent indicator basis for regional studies of climate extremes [3]. The availability of global datasets based on extreme climate indices has also made it possible to compare changes in climate extremes across different regions [4]. In China, changes in climate extremes are mainly reflected in pronounced warming and an enhancement of precipitation extremes, including upward trends in heat-related metrics and downward trends for cold-associated events, and these changes are closely linked to large-scale atmospheric circulation backgrounds [5,6]. The Yangtze River Basin includes multiple geomorphic and climatic zones, such as the northeastern Tibetan margin, Sichuan lowlands, and the middle-lower alluvial plains, and the humid eastern sector of China. Spatial contrasts in elevation, landform structure, and heat-water conditions contribute to regional heterogeneity in temperature extremes, precipitation extremes, and compound drought-heatwave events within the basin [7–9], making it a typical region for studying extreme climate change and its ecological effects.

The normalized difference vegetation index (NDVI) is widely used to characterize vegetation cover, canopy activity, and ecosystem dynamics, and remains a key remote-sensing metric for long-term vegetation monitoring [10,11]. Long-term NDVI datasets provide an important basis for analyzing vegetation dynamics since the 1980s. Because long-term NDVI products may yield different estimates of vegetation trends, temporal continuity and cross-sensor consistency are important considerations in multi-decadal vegetation

analyses [12,13]. Previous studies have identified widespread greening tendency in global vegetation, and vegetation changes are jointly driven by CO_2 fertilization, climatic variation, land-use change, and ecological restoration projects [14]. In China, vegetation NDVI changes show significant spatial heterogeneity, with clear differences among regions, topographic settings, and vegetation types. At the national scale, vegetation greening reflects the combined influence of climatic fluctuations and human interventions [15,16]. Across the Yangtze River Basin, vegetation cover has generally increased, although localized fluctuations or degradation remain evident in upper-reach high-elevation zones, urbanized lower-reach areas, and some ecologically fragile regions [17]. Vegetation restoration within the basin is shaped by climate change, anthropogenic disturbance, and ecological management, while vegetation sensitivity to climatic fluctuations shows regional differences [18,19]. Interannual vegetation responses to climate factors vary across geomorphic zones in the Yangtze River Basin, further indicating that vegetation change has clear spatial differentiation within the basin [20].

Vegetation NDVI is closely regulated by climatic change. Temperature and precipitation can influence vegetation growth by altering thermal conditions, water supply, and growing-season length [21]. However, vegetation responses to climate drivers vary among vegetation types in both direction and strength, and precipitation anomalies may affect vegetation growth with a delayed response rather than only during the same period [22,23]. Extreme climate events may cause more abrupt ecological effects than mean climate variations. For example, heat extremes can reduce vegetation activity by increasing evapotranspiration and drought stress, whereas heavy precipitation may either relieve water limitation through soil-moisture recharge or damage vegetation through waterlogging and runoff disturbance [24]. Within the Yangtze River Basin, extreme hydrometeorological events influence vegetation differently across regions. Evidence from Southwest China further suggests that local hydrothermal conditions and vegetation composition can shape how ecosystems respond to climate extremes [25,26]. In addition, vegetation responses to climate change are not always synchronous. Antecedent climate conditions can affect current vegetation growth through soil moisture, phenological processes, and ecosystem memory [27,28]. Lag and accumulation processes therefore need to be considered when interpreting climate–vegetation relationships. National-scale evidence has demonstrated that vegetation growth responds to both mean and extreme hydrothermal conditions through delayed and cumulative pathways [29,30].

Recent studies have extended this line of inquiry by assessing lagged associations between vegetation and climate extremes across China [31], drought-related cumulative and lagged responses in the upper Yangtze River Basin [32], and extreme-climate response windows in the Poyang Lake wetland [33]. Two newly published studies have further investigated ETCCDI-based relationships between extreme climate indices and NDVI and the cumulative and lagged climatic associations with vegetation phenology across the Yangtze River Basin [34,35]. However, earlier basin-wide studies largely focused on mean climatic variability or general vegetation trends [18–20], whereas the recent studies summarized above address national-scale patterns, individual subregions, drought, phenology, or periods beginning after 2000. Long-term evidence extending back to the early 1980s remains limited, particularly regarding systematic comparisons of optimal lagged cumulative association windows among major vegetation types. Accordingly, the primary objective of this study was to quantify the temporal trends and spatial patterns of 15 extreme climate indices and vegetation NDVI across the Yangtze River Basin during 1982–2022. The secondary objective was to evaluate NDVI–extreme-climate correlations and identify optimal lagged cumulative association windows across the upper, middle, and lower reaches and among five major vegetation types.

2. Materials and Methods

2.1. Study Area

The Yangtze River Basin (YRB) lies across a broad east–west transect of China, covering parts of southwestern, central, and eastern China. It is an important ecological barrier and a climate-change-sensitive region in China. Geographically, the basin ranges from approximately 90°33′E to 122°25′E and 24°30′N to 35°45′N (Figure 1a), covering about 1.8 million km^2. The main stream is about 6300 km long. Elevation decreases from west to east, with landforms shifting from the Tibetan Plateau and Hengduan Mountains toward the Sichuan Basin, Jianghan Plain, Dongting Lake Plain, Poyang Lake Plain, and finally the Yangtze River Delta. This topographic transition produces complex terrain gradients and spatial differentiation in hydrothermal conditions [36]. The interaction between monsoonal climate and complex terrain produces marked regional contrasts in temperature, precipitation, and vegetation growth conditions across the YRB. Hydroclimatically, precipitation is strongly seasonal under the influence of the East Asian monsoon, with most rainfall occurring during the warm season. The upper reaches are generally characterized by colder, high-elevation conditions, whereas the middle and lower reaches have warmer and more humid climates with a more pronounced monsoonal rainfall regime. Together, these hydroclimatic contrasts contribute to spatially heterogeneous patterns of vegetation-cover change and vegetation responses to climate across the basin [19]. For regional comparison, the YRB was separated into upper, middle, and lower reaches (Figure 1c). The upper reach was defined as the area upstream of Yichang, the middle reach as the area from Yichang to Hukou, and the lower reach as the area downstream of Hukou. Vegetation types are diverse within the basin, including grassland, meadow, alpine vegetation, cultivated vegetation, forest, and shrubland communities. Based on vegetation distribution characteristics and sample representativeness, this study focused on five vegetation types: cultivated vegetation, shrubland, coniferous forest, broadleaf forest, and grassland (Figure 1b). Earlier work has reported substantial spatiotemporal differences in YRB vegetation greenness, which is jointly controlled by climate, topography, and human activities [37].

2.2. Data Sources and Processing

This study involved three datasets: gridded meteorological observations, NDVI observations, and vegetation-type information. Meteorological variables were obtained from CN05.1, a station-based daily gridded observational dataset released by the Climate Change Research Center, Institute of Atmospheric Physics, Chinese Academy of Sciences (https://nzc.iap.ac.cn/content?aid=999&cid=24 accessed on 11 March 2026). CN05.1 was generated from daily observations at 2416 meteorological stations across China using anomaly-based interpolation [38]. The version used in this study covers 1961–2022 at a daily temporal resolution and a spatial resolution of 0.25° × 0.25° (approximately 25 km). Daily precipitation, daily maximum temperature, and daily minimum temperature were used as inputs for calculating the extreme climate indices. In ArcGIS 10.7 (ESRI, Redlands, CA, USA), the three daily meteorological variables were transformed from raster layers into point-based series for each grid cell. These series were exported as TXT files and processed in RClimDex 2.0 to calculate the extreme climate indices. RClimDex 2.0 is an R-based package developed under the ETCCDI framework for quality checking daily temperature and precipitation inputs and computing standardized climate-extreme indices from daily meteorological records. The output indices were interpolated bilinearly to 1/12° (approximately 0.083°, or about 8–9 km), the same grid spacing as the NDVI product, to ensure consistency in pixel-scale spatiotemporal analyses.

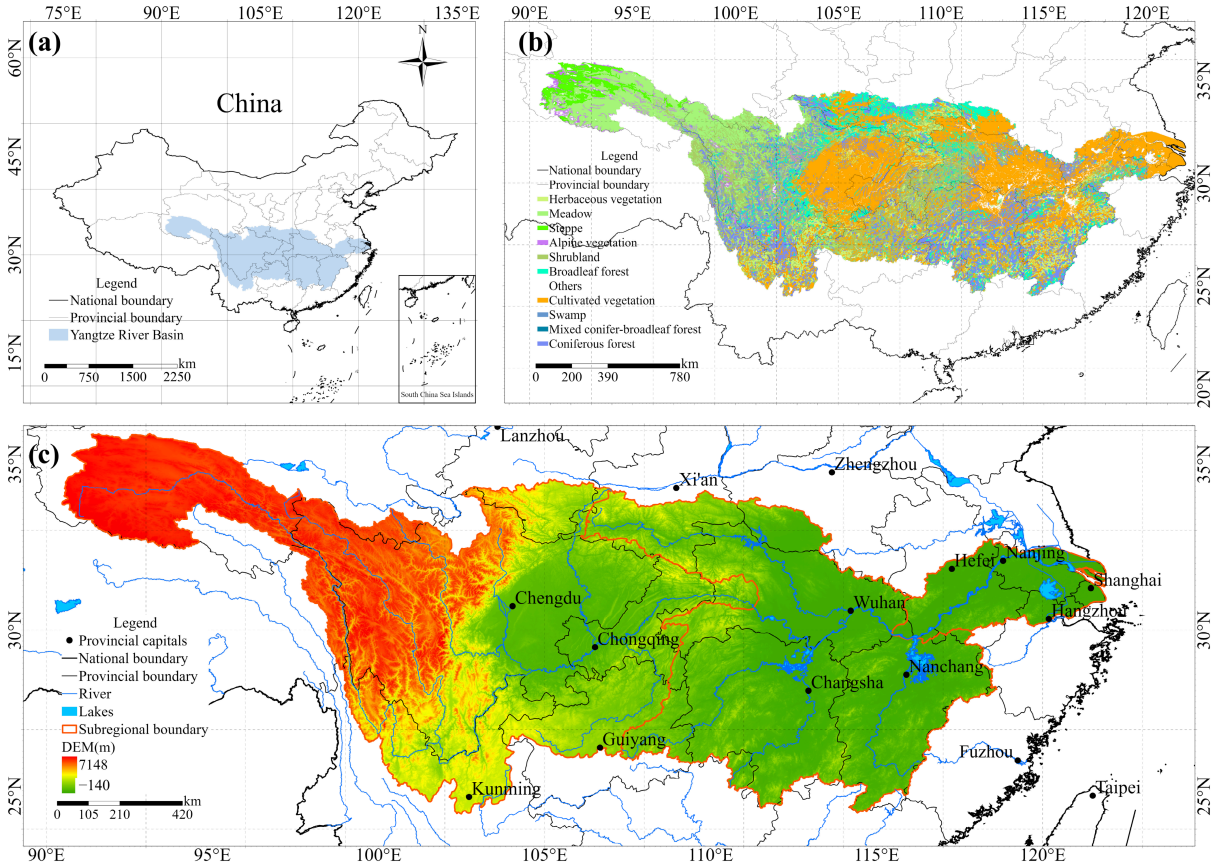


Figure 1. Study area and spatial datasets: (**a**) geographic position of the Yangtze River Basin in China; (**b**) vegetation-type distribution; and (**c**) elevation and main river network.

Vegetation greenness was represented by PKU-GIMMS NDVI V1.2 (Peking University, Beijing, China), a satellite-derived global NDVI product developed by a Peking University research team [12]. This product provides a spatially and temporally harmonized NDVI record covering the entire 1982–2022 study period at a spatial resolution suitable for basin-scale analysis. The product was reconstructed from the AVHRR-based GIMMS NDVI3g (NASA Goddard Space Flight Center, Greenbelt, MD, USA) record using Landsat NDVI reference samples and was subsequently consolidated with MODIS NDVI to improve temporal consistency and extend the record to 2022. It provides half-monthly observations from 1982 to 2022 at a spatial resolution of 1/12° (approximately 8–9 km). Each original file contains two bands: an NDVI band and a corresponding quality-control (QC) band. After the data were clipped to the Yangtze River Basin, the integer NDVI values were converted using the scale factor of 0.001. Because the QC coding differs between the AVHRR-based period (1982–2002) and the MODIS-consolidated period (2003–2022), period-specific quality screening was applied. Pixels potentially affected by snow or clouds during 1982–2002 and pixels affected by snow or ice during 2003–2022 were set to NoData. The fill value of 65,535 and scaled NDVI values below 0.10 were also excluded. Monthly NDVI was calculated pixel by pixel using the maximum-value composite of the two half-monthly NDVI observations within each month. For each year, the annual NDVI metric used in this study was calculated as the maximum of the monthly NDVI values from April to October. Annual NDVI was used for trend and spatial-change analyses, whereas monthly NDVI was used for lagged cumulative correlation analysis with extreme climate indices. Meteorological records were restricted to 1982–2022 to match the NDVI period. The NDVI product was accessed through Zenodo (https://zenodo.org).

Vegetation-type information was based on the 1:1,000,000 Vegetation Map of China, which was compiled by the Editorial Committee of the Vegetation Map of China, Chinese Academy of Sciences [39], and distributed by the National Cryosphere Desert Data Center (https://www.ncdc.ac.cn). These data provided the basis for identifying major vegetation categories within the study area. The original vegetation map was resampled to 1/12° with nearest-neighbor interpolation. This approach preserved categorical vegetation labels, but target grid cells located near vegetation-type boundaries may contain mixed vegetation signals or be sensitive to the spatial alignment between the vegetation map and the NDVI grid. According to the dominant vegetation composition and sample representativeness within the basin, vegetation was reclassified into five main categories: cultivated vegetation, shrubland, coniferous forest, broadleaf forest, and grassland. This static vegetation map was used only to stratify the NDVI analysis by vegetation type and was not used to characterize interannual land-use or land-cover changes.

Extreme climate indices were calculated using daily maximum temperature, daily minimum temperature, and precipitation as input variables in RClimDex 2.0, following the core-index framework of the Expert Team on Climate Change Detection and Indices (ETCCDI) [3]. Accordingly, the 10th/90th percentile thresholds used for TN10p, TN90p, TX10p, and TX90p were retained as standard ETCCDI definitions rather than optimized thresholds selected specifically for this study, ensuring consistency with internationally comparable climate-extreme indices. Because this study emphasizes climate extremes and their relationships with vegetation NDVI, the selected indices also needed to reflect the climatic features of the Yangtze River Basin and provide representative information on regional extreme events. Therefore, we retained 15 indices for analysis: nine temperature-related indices and six precipitation-related indices. Table 1 summarizes the definitions and units of these indices.

Table 1. Extreme climate indices analyzed in this study.

Index Category	Index Code	Index Description	Unit
Extreme temperature indices	TN10p	Cold nights: days with daily minimum temperature lower than the 10th-percentile threshold	days
	TN90p	Warm nights: days with daily minimum temperature higher than the 90th-percentile threshold	days
	TX10p	Cold days: days with daily maximum temperature lower than the 10th-percentile threshold	days
	TX90p	Warm days: days with daily maximum temperature higher than the 90th-percentile threshold	days
	TNn	Monthly minimum of daily minimum temperature	°C
	TNx	Monthly maximum of daily minimum temperature	°C
	TXn	Monthly minimum of daily maximum temperature	°C
	TXx	Monthly maximum of daily maximum temperature	°C
	DTR	Diurnal temperature range: difference between daily maximum and minimum temperature within a year	°C

Table 1. *Cont.*

Index Category	Index Code	Index Description	Unit
Extreme precipitation indices	CDD	Consecutive dry days: longest dry spell with daily precipitation below 1 mm	days
	CWD	Consecutive wet days: longest wet spell with daily precipitation at or above 1 mm	days
	R95p	Heavy precipitation amount: annual precipitation total from days above the 95th-percentile threshold	mm
	R99p	Very heavy precipitation amount: annual precipitation total from days above the 99th-percentile threshold	mm
	RX1day	Monthly maximum 1-day precipitation amount	mm
	RX5day	Monthly maximum consecutive 5-day precipitation amount	mm

2.3. Methods

The full 1982–2022 record was used in all statistical analyses, providing 41 annual observations for trend and annual correlation analyses and up to 492 monthly observations for lag–accumulation analysis before window construction. Uncertainty and statistical robustness were evaluated using confidence intervals, bootstrap resampling, partial correlation analysis, and multiple-testing correction where appropriate.

2.3.1. Trend Analysis and Significance Testing

For 1982–2022, trends in NDVI and extreme climate indices over the Yangtze River Basin were evaluated using two nonparametric methods. Specifically, the Sen's slope estimator was adopted to determine whether each variable showed an increasing or decreasing tendency and to quantify the corresponding rate of change. The statistical reliability of these tendencies was then evaluated with the M-K nonparametric test [40]. Sen's slope is less affected by extreme values and is therefore appropriate for detecting monotonic trends in long-term climate and vegetation records. The estimator is expressed as follows:

$$\beta = Median\left(\frac{x_j - x_i}{j - i}\right),\ 1 \le i < j \le n \tag{1}$$

where β denotes the rate of change estimated from all pairwise combinations in the time series; x_i and x_j denote the corresponding NDVI or extreme climate index values for years i and j and n represents the full length of the study period. Positive β, values indicate upward changes, whereas negative values indicate downward changes. For decadal-scale interpretation, the annual slope was multiplied by 10:

$$Slope = 10\beta \tag{2}$$

Trend significance was evaluated using the M-K test. The standardized Z statistic indicates both trend direction and statistical significance. An upward trend is identified when Z is positive, whereas a downward trend is identified when Z is negative. Trends were considered significant at $p < 0.05$ when $|Z|$ exceeded 1.96. To control false discoveries arising from multiple grid-cell-level trend tests, the Benjamini–Hochberg false discovery rate (FDR) correction was applied to the corresponding M-K p values. For the extreme-temperature and extreme-precipitation indices, all valid grid-cell p values were jointly adjusted within each index group, whereas the NDVI grid-cell p values were adjusted

separately. Spatial trends with FDR-adjusted q values below 0.05 were considered statistically significant [41,42]. For regional-average series, possible change points were examined using the sequential M-K procedure. Abrupt-change timing was inferred from the crossing point between the forward UF curve and backward UB curve. The ± 1.96 boundary was adopted as the 0.05-level threshold. To quantify the uncertainty of the trend estimates, 95% confidence intervals were calculated for Sen's slope estimates.

2.3.2. Correlation Analysis

To determine whether vegetation changes were linked to variations in climate extremes, Pearson's correlation coefficient was calculated for each NDVI-index pair [43]. The formula used for this analysis is given as follows:

$$r = \frac{\sum_{i-1}^{n} (x_i - \overline{x})(y_i - \overline{y})}{\sqrt{\sum_{i=1}^{n} (x_i - \overline{x})^2} \sqrt{\sum_{i=1}^{n} (y_i - \overline{y})^2}} \quad (3)$$

where x_i denotes one annual value from an extreme climate index, y_i denotes the corresponding NDVI value, $\overline{x}$ and $\overline{y}$ denote the average values of the climate-index and NDVI series, respectively, and r is used to measure their linear relationship. A coefficient above zero means that NDVI and the climate index tend to vary in the same direction, whereas a coefficient below zero means that they tend to vary in opposite directions. The magnitude of $|r|$ reflects the strength of the association. The correlation calculation was first performed at the basin scale and was subsequently extended to the three subregions and different vegetation categories. For each individual correlation test, $p < 0.05$ represented nominal statistical significance. To control false discoveries arising from multiple correlation tests, the Benjamini–Hochberg FDR correction was applied separately to the basin/reach analysis and the vegetation-type analysis. Correlations with FDR-adjusted q values below 0.05 were considered statistically significant.

For the key annual NDVI–climate correlations at the basin, subregional, and vegetation-type scales, 95% confidence intervals were estimated using a three-year moving block bootstrap to account for short-term temporal dependence in the time series. Partial correlation analysis was further conducted for the key annual NDVI–extreme climate relationships by controlling for annual mean temperature and annual precipitation. Specifically, both NDVI and each extreme climate index were first regressed against annual mean temperature and annual precipitation, and the Pearson correlation between the resulting residuals was then calculated [44].

2.3.3. Lagged Cumulative Correlation Analysis

Considering that vegetation responses to climatic conditions may exhibit both lagged and cumulative characteristics [29,30], extreme climate index series were constructed for different lag–accumulation (LA) combinations using the original monthly data, and their Pearson correlation coefficients with monthly NDVI were calculated. Let $NDVI_t$ denote the NDVI value in month t, and let X_t denote the extreme climate index value in the corresponding month. The climate index associated with a given LA combination was calculated as follows:

$$X_{t,L,A} = \begin{cases} \frac{1}{A+1} \sum_{i=0}^{A} X_{t-L-i} \\ \sum_{i=0}^{A} X_{t-L-i} \end{cases} \quad (4)$$

where $X_{t,L,A}$ denotes the transformed climate index corresponding to $NDVI_t$. L specifies the starting lag, that is, the number of months between the NDVI month and the most recent climate month included in the window. A specifies the number of additional

preceding months included from that starting month. Therefore, each LA window contains $A+1$ monthly climate values, extending from $t-L$ to $t-L-A$. For example, L0A0 includes only the current month; L0A3 includes the current month and the preceding three months; and L1A2 includes the three months from $t-1$ to $t-3$, with the window ending one month before the NDVI month. DTR and extreme temperature indices were averaged within each window, whereas RX1day and RX5day were summed.

Four lag levels ($L = 0,1,2,3$) and four accumulation levels ($A = 0,1,2,3$) were considered, subject to $L + A \leq 3$. Accordingly, ten LA combinations were tested: L0A0, L1A0, L2A0, L3A0, L0A1, L0A2, L0A3, L1A1, L1A2, and L2A1. Combinations with $L = 0$ and $A > 0$ represent cumulative windows, those with $L > 0$ and $A = 0$ represent lagged responses, and those with $L > 0$ and $A > 0$ represent combined lagged cumulative responses. For each grid cell or regional vegetation type, the optimal LA window was selected as the window with the maximum absolute Pearson correlation coefficient. Because ten candidate LA windows were tested for each NDVI–climate pair, Benjamini–Hochberg false discovery rate (FDR) correction was applied to evaluate the influence of multiple testing on statistical significance.

$$r_{L,A} = corr(NDVI_t, X_{t,L,A}) \tag{5}$$

Pearson's correlation coefficient was calculated separately for each of the ten LA combinations at each pixel. The combination yielding the largest absolute correlation coefficient was identified as the optimal LA type:

$$(L^*, A^*) = \max|r_{L,A}| \tag{6}$$

where L^* and A^* denote the optimal lag and accumulation parameters, respectively. Thus, the optimal LA type represents the tested temporal window showing the strongest correlation between NDVI and the corresponding extreme climate index.

3. Results

3.1. Spatiotemporal Variation Characteristics of Extreme Climate Indices

3.1.1. Temporal Variation Characteristics of Extreme Climate Indices

During 1982–2022, basin-wide temperature-extreme indices displayed a warming-dominated evolution (Figure 2), characterized by fewer cold events and more warm events. Cold-night days (TN10p) and cold-day days (TX10p) declined at rates of −9.7 days per decade and −6.3 days per decade (Figure 2a,c), respectively, showing a sustained reduction in low-temperature extremes. In contrast, TN90p and TX90p rose substantially, with rates of 11.7 days per decade and 10.2 days per decade (Figure 2b,d), respectively, reflecting a marked increase in high-temperature extremes. The four temperature-intensity indices, TNn, TNx, TXn, and TXx, also showed upward trends, with rates of 0.20, 0.34, 0.24, and 0.41 °C per decade (Figure 2e–h), respectively. Among them, TXx showed a relatively larger increase (Figure 2h), indicating that the enhancement of extreme maximum temperature was more pronounced. DTR changed only slightly, increasing by 0.03 °C per decade (Figure 2i), indicating little overall change in the diurnal temperature range. The M-K curves suggest that after around 2000, UF values for cold-related indices generally declined, while those of warm indices continued to rise. Some indices exceeded the significance threshold in the later period, further indicating that extreme temperature change across the basin showed a staged strengthening pattern.

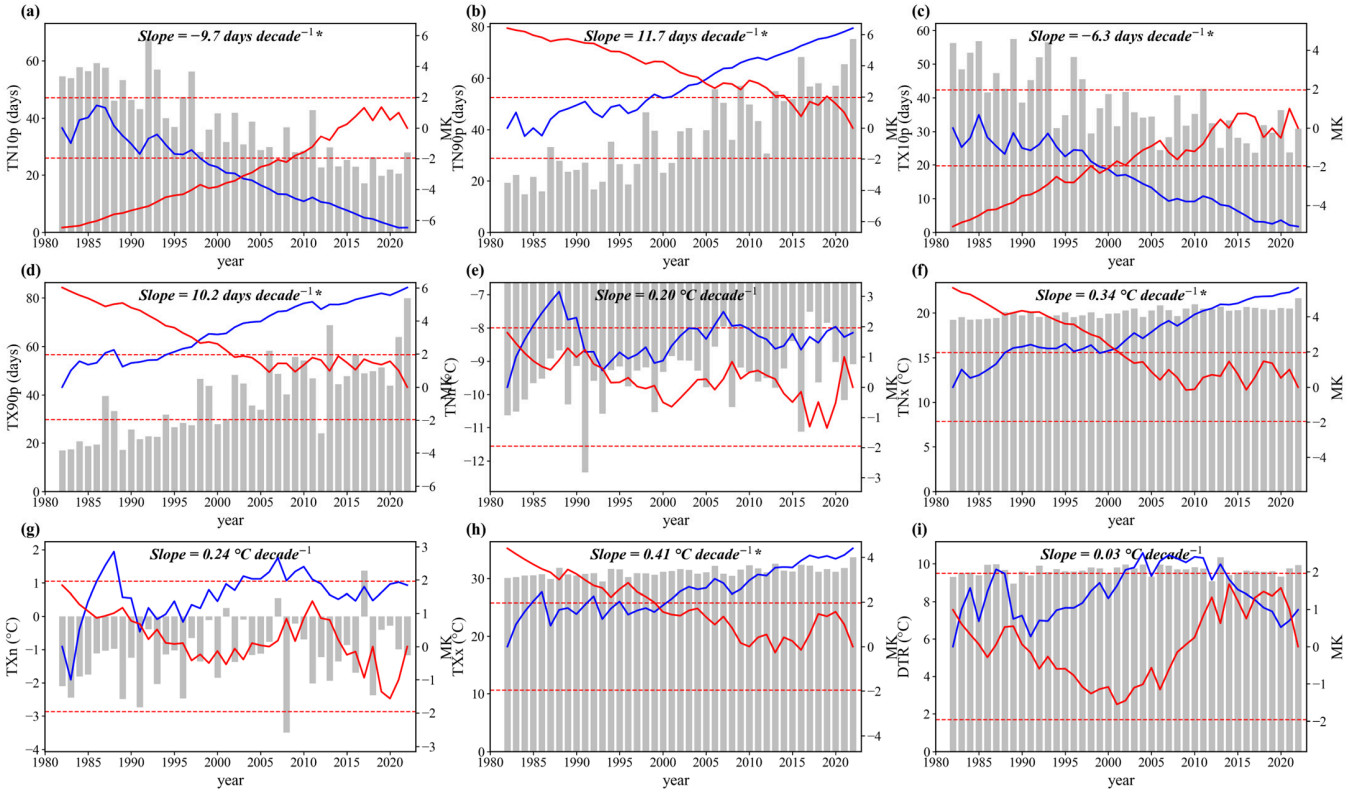


Figure 2. Temporal changes in extreme temperature indices across the Yangtze River Basin: (**a**) TN10p, (**b**) TN90p, (**c**) TX10p, (**d**) TX90p, (**e**) TNn, (**f**) TNx, (**g**) TXn, (**h**) TXx, and (**i**) DTR. Bars show annual index values; blue and red curves denote UF and UB statistics from the M-K test, respectively; red dashed lines indicate the ±1.96 significance threshold. Slope values are expressed per decade. An asterisk following a slope value indicates a statistically significant temporal trend according to the M-K test ($p < 0.05$).

Precipitation-extreme indices tended to increase overall, although the magnitude varied among indices (Figure 3). CDD and CWD rose slightly, at rates of 0.07 days per decade and 0.25 days per decade (Figure 3a,b), respectively, both indicating weak increases and suggesting that changes in dry and wet persistence across the basin were not strong. In contrast, heavy-precipitation-related indices increased more noticeably. R95p and R99p increased at rates of 9.2 mm per decade and 5.6 mm per decade (Figure 3c,d), respectively, suggesting greater contributions from heavy and very heavy precipitation events. RX1day and RX5day also followed upward trajectories, with corresponding increases of 0.8 mm per decade and 2.1 mm per decade (Figure 3e,f), respectively, indicating increases in both the annual strongest 1-day rainfall event and the maximum rainfall accumulated over five consecutive days. The M-K curves show that R95p, R99p, RX1day, and RX5day mostly shifted toward increasing tendencies in the later study period, with a clearer strengthening signal after 2010. In contrast, CDD and CWD showed large interannual fluctuations, and their abrupt-change signals were relatively unstable. Overall, extreme precipitation change across the basin was mainly reflected by intensified heavy precipitation, whereas changes in persistent dry and wet events were relatively weak.

To quantify the uncertainty of the temporal trend estimates for both extreme climate indices and NDVI, Sen's slope estimates and their 95% confidence intervals are summarized in Table 2.

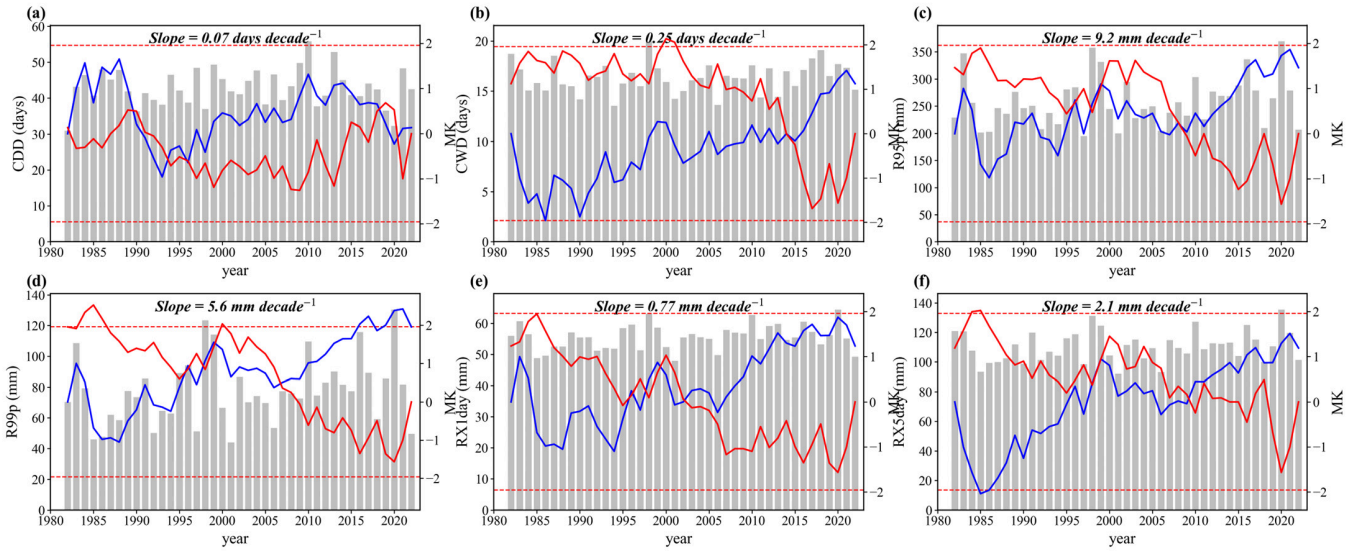


Figure 3. Temporal changes in extreme precipitation indices across the Yangtze River Basin: (**a**) CDD, (**b**) CWD, (**c**) R95p, (**d**) R99p, (**e**) RX1day, and (**f**) RX5day. Bars show annual index values; blue and red curves denote UF and UB statistics from the M-K test, respectively; red dashed lines indicate the ±1.96 significance threshold. Slope values are expressed per decade.

Table 2. Sen's slope estimates and 95% confidence intervals for NDVI and extreme climate indices during 1982–2022.

Variable	Unit	Basin	Upper	Middle	Lower
NDVI	decade^{-1}	0.0038 [0.0023, 0.0058] *	0.0022 [0.0005, 0.0047] *	0.0069 [0.0049, 0.0092] *	0.0020 [−0.0014, 0.0054]
TN10p	days decade^{-1}	−9.66 [−11.07, −7.81] *	−10.14 [−12.12, −7.85] *	−8.74 [−10.59, −6.57] *	−9.45 [−12.09, −6.36] *
TN90p	days decade^{-1}	11.62 [9.41, 14.01] *	11.74 [9.83, 13.87] *	11.09 [8.53, 13.71] *	12.11 [9.39, 15.31] *
TX10p	days decade^{-1}	−6.20 [−7.95, −4.20] *	−7.53 [−9.53, −5.54] *	−3.90 [−6.76, −1.67] *	−5.96 [−9.39, −2.40] *
TX90p	days decade^{-1}	10.21 [8.05, 12.48] *	10.59 [8.20, 13.49] *	9.89 [7.08, 12.68] *	10.14 [6.84, 13.34] *
TNn	°C decade^{-1}	0.20 [−0.01, 0.45]	0.36 [0.12, 0.62] *	0.01 [−0.29, 0.33]	0.17 [−0.27, 0.67]
TNx	°C decade^{-1}	0.34 [0.26, 0.42] *	0.38 [0.29, 0.45] *	0.29 [0.17, 0.39] *	0.40 [0.23, 0.57] *
TXn	°C decade^{-1}	0.24 [−0.02, 0.49]	0.22 [−0.05, 0.50]	0.18 [−0.10, 0.51]	0.16 [−0.27, 0.56]
TXx	°C decade^{-1}	0.41 [0.25, 0.58] *	0.47 [0.30, 0.63] *	0.32 [0.11, 0.54] *	0.39 [0.09, 0.69] *
DTR	°C decade^{-1}	0.03 [−0.04, 0.11]	0.04 [−0.04, 0.12]	0.03 [−0.07, 0.13]	0.05 [−0.04, 0.14]
CDD	days decade^{-1}	0.07 [−1.41, 1.69]	0.74 [−1.62, 3.23]	−0.36 [−1.65, 0.92]	−1.17 [−2.93, 0.54]
CWD	days decade^{-1}	0.26 [−0.23, 0.61]	0.29 [−0.31, 0.88]	0.06 [−0.30, 0.41]	0.12 [−0.31, 0.45]
R95p	mm decade^{-1}	9.20 [−2.67, 19.58]	2.92 [−2.45, 9.50]	13.56 [−7.05, 33.10]	17.77 [−12.54, 46.04]
R99p	mm decade^{-1}	5.02 [−0.30, 10.37]	1.02 [−2.56, 4.56]	9.14 [−1.32, 17.63]	9.47 [−3.99, 22.99]
RX1day	mm decade^{-1}	0.76 [−0.41, 1.92]	0.07 [−0.76, 0.98]	1.53 [−0.66, 3.20]	3.08 [−0.74, 6.79]
RX5day	mm decade^{-1}	1.97 [−1.45, 4.97]	0.21 [−1.44, 2.10]	3.37 [−2.12, 7.90]	5.72 [−3.80, 15.33]

Note: Values are Sen's slopes per decade, with 95% confidence intervals in brackets. NDVI is dimensionless; other units follow the definitions of the corresponding indices. Asterisks indicate that the 95% confidence interval excludes zero.

3.1.2. Spatial Variation Characteristics of Extreme Climate Indices

The spatial maps of temperature extremes reveal a basin-wide shift from fewer cold extremes to more warm extremes (Figure 4). This pattern suggests coherent warming-related changes across the study area. TN10p and TX10p were both dominated by negative trends, with regional mean change rates of −9.4 days per decade and −6.1 days per decade (Figure 4a,c), respectively. This result points to a broad reduction in cold-night and cold-day occurrence. In contrast, TN90p and TX90p showed basin-wide positive changes, with average change rates of 11.6 days per decade and 10.4 days per decade (Figure 4b,d), respectively. These positive slopes indicate more frequent warm nights and warm days in all three river reaches.

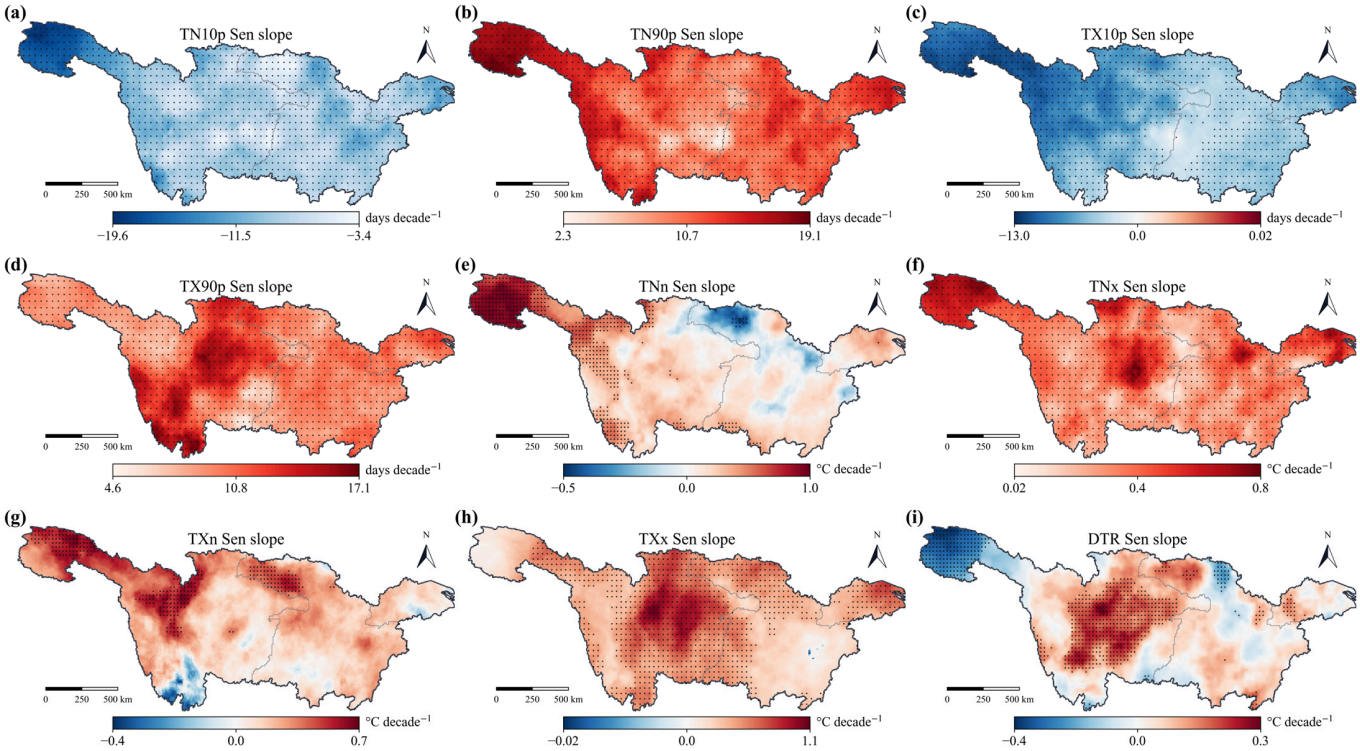


Figure 4. Spatial distribution of Sen's slope for extreme temperature indices: (**a**) TN10p, (**b**) TN90p, (**c**) TX10p, (**d**) TX90p, (**e**) TNn, (**f**) TNx, (**g**) TXn, (**h**) TXx, and (**i**) DTR. Slope values are expressed per decade, with units shown in the corresponding color bars. Stippling, regularly thinned for visual clarity, indicates grid cells with statistically significant trends after the Benjamini–Hochberg FDR correction ($q < 0.05$).

The strongest warm-index increases appeared mainly in the western, northern, and locally central basin, showing that high-temperature extremes intensified unevenly across space. TNx, TXn, TXx, and TNn further showed that extreme temperature levels generally increased (Figure 4e–h). Among these indices, the mean trends of TNx and TXx reached 0.35 and 0.41 °C per decade, respectively. TXx increased more strongly in all three river reaches, revealing regional contrasts in high-temperature intensification. Although TNn increased overall, weak decreases occurred in some north-central and eastern local areas, suggesting that the spatial response of low-temperature extremes was more complex. Pixels with positive and negative DTR trends accounted for 71.8% and 28.1%, respectively, and were spatially interlaced (Figure 4i), indicating that daily high-temperature and low-temperature variations did not occur at the same pace. Overall, temperature-extreme changes in the study area were mainly expressed as a reduction in cold extremes accompanied by an intensification of warm extremes, with spatial differences among individual temperature indices. Across the nine temperature indices, 96.6% of the grid-cell tests that were nominally significant remained significant after the FDR correction, indicating that the dominant spatial patterns of fewer cold extremes and more intense warm extremes were robust to multiple-testing control.

Extreme precipitation indices showed stronger spatial heterogeneity than temperature indices (Figure 5). Persistence-related indices changed weakly, whereas heavy-precipitation-related indices increased more noticeably. The regional mean change rates of CDD and CWD were 0.14 days per decade and 0.17 days per decade (Figure 5a,b), respectively, indicating small overall changes. Pixel statistics showed that positive and negative trend pixels accounted for 39.0% and 56.8% for CDD, and 51.5% and 39.5% for CWD, respectively, indicating that consecutive dry and wet processes did not show consistent basin-wide

changes. Positive CDD slopes were concentrated in the western and southwestern basin, whereas weak negative slopes were more common in the central and eastern areas. CWD appeared as scattered patches, indicating strong local controls on consecutive wet processes.

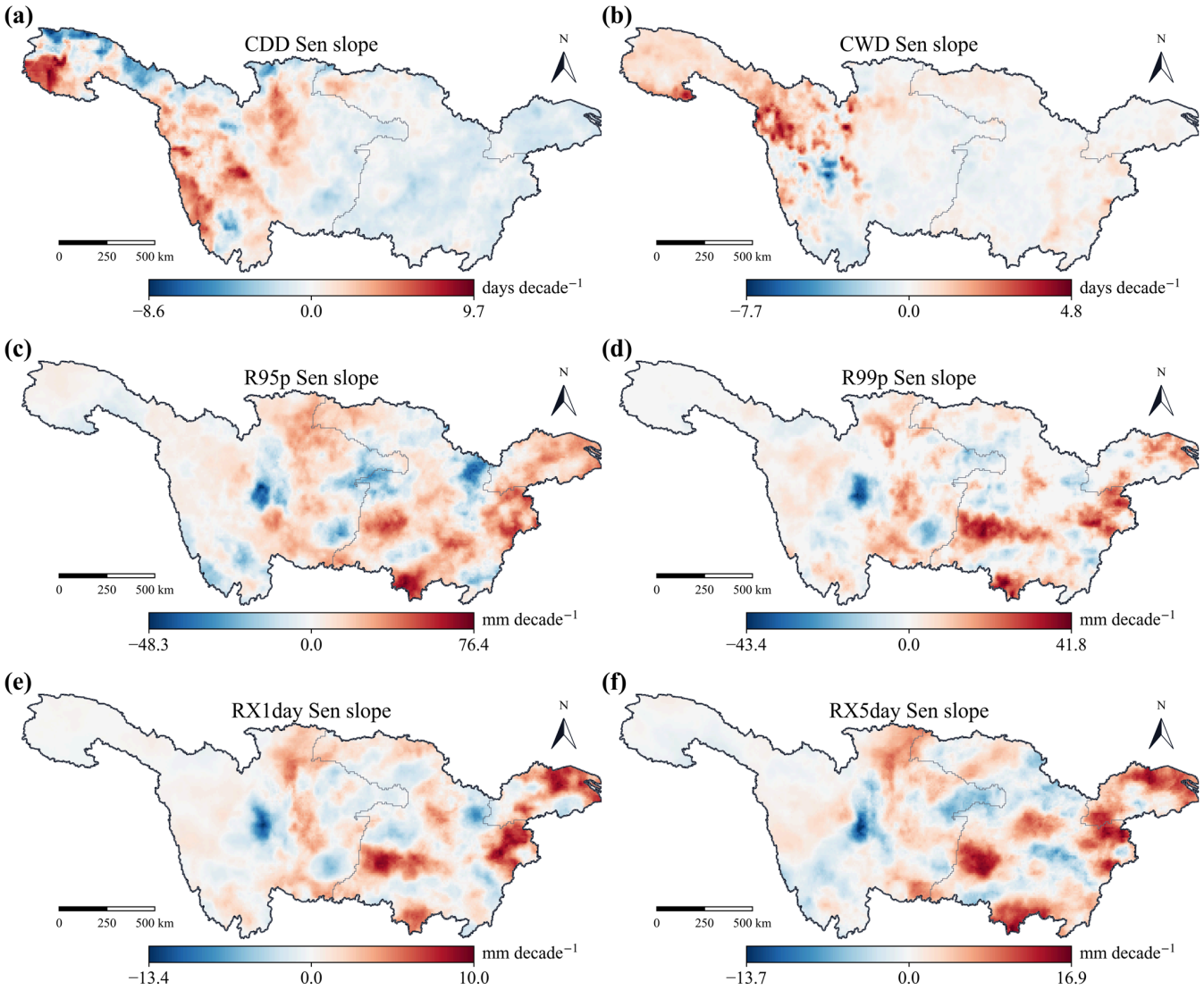


Figure 5. Spatial distribution of Sen's slope for extreme precipitation indices: (**a**) CDD, (**b**) CWD, (**c**) R95p, (**d**) R99p, (**e**) RX1day, and (**f**) RX5day. Slope values are expressed per decade, with units shown in the corresponding color bars. No grid-cell-level trends remained statistically significant after the Benjamini–Hochberg FDR correction ($q < 0.05$).

In contrast, R95p, R99p, RX1day, and RX5day showed positive slopes across most pixels (Figure 5c–f). R95p increased by 7.1 mm per decade on average, and 69.7% of pixels had positive slopes. R99p increased by 2.8 mm per decade; positive slopes covered 52.3% of pixels. These positive Sen's slope patterns indicate an overall tendency toward increasing heavy and very heavy precipitation, although R99p showed more pronounced spatial differentiation. RX1day increased by 0.6 mm per decade, with positive slopes covering 64.0% of pixels. RX5day increased by 1.5 mm per decade, and 61.8% of pixels were positive. Both the single-day and 5-day precipitation extremes were dominated by positive Sen's slopes, with the multi-day accumulation index showing the larger estimated increase. The lower reaches and the eastern-southeastern basin had the strongest strengthening of heavy precipitation. R95p increased by 3.4 mm per decade in the upper reaches, 10.7 mm per decade in the middle reaches, and 17.9 mm per decade in the lower reaches. RX5day

increased by 0.4, 2.4, and 6.0 mm per decade in all three river reaches, respectively. Overall, precipitation-extreme changes were mainly reflected in stronger heavy-precipitation totals and enhanced multi-day precipitation accumulation, while persistence indices, including CDD and CWD, changed only slightly. Spatially, the eastern basin and lower reaches showed the clearest increase in heavy-precipitation exposure. Across the six extreme precipitation indices, 5.6% of the valid grid-cell tests met the unadjusted $p < 0.05$ threshold, but none remained significant after the FDR correction. Therefore, these maps primarily characterize the spatial direction and magnitude of the estimated changes rather than statistically robust local trends.

3.2. Spatiotemporal Variation Characteristics of Vegetation NDVI

3.2.1. Temporal Variation Characteristics of Vegetation NDVI

Over the 1982–2022 study period, the vegetation canopy across the Yangtze River Basin exhibited a broad greening pattern, indicating increased vegetation greenness. The basin-wide NDVI increased at a rate of 0.0038 per decade, with the change being statistically significant ($p < 0.05$), suggesting that vegetation growth conditions have continuously improved over the past 40 years. Among the three river reaches, the middle reaches maintained the highest NDVI, generally above 0.75, and increased significantly by 0.0069 per decade. This indicates the strongest greening among the three reaches. NDVI in the upper reaches was relatively low, mostly fluctuating between 0.69 and 0.72, with a modest rate of 0.0022 per decade, indicating a relatively small improvement. In the lower reaches, NDVI was between the basin-wide value and the middle-reach value, with relatively strong interannual fluctuations and a slope of 0.0020 per decade, reflecting a weak but positive NDVI tendency. The multi-year mean NDVI map in Figure 6a was calculated by averaging the valid annual NDVI values at each pixel over 1982–2022, while Figure 6b summarizes the annual NDVI series for the whole basin and the three river reaches.

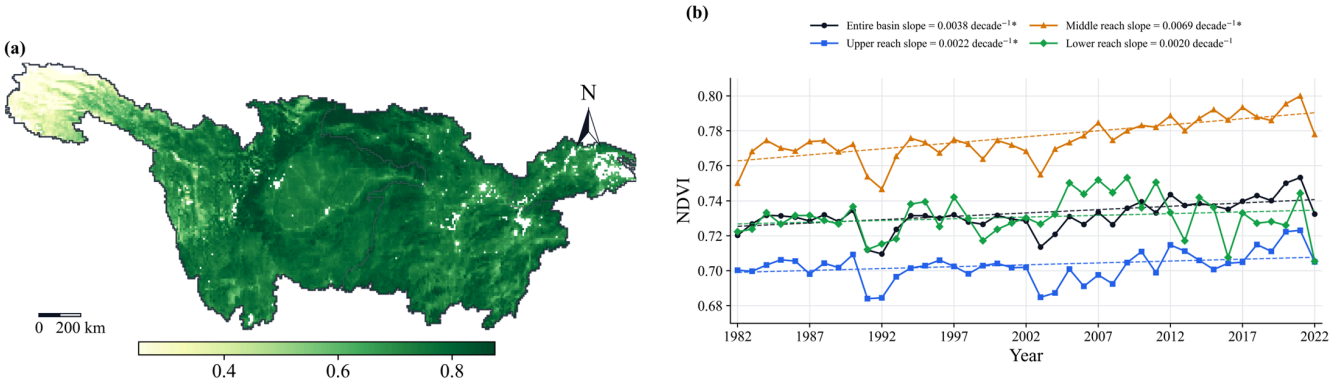


Figure 6. Spatial distribution and temporal variation of NDVI in the Yangtze River Basin from 1982 to 2022: (**a**) multi-year mean NDVI; (**b**) interannual NDVI variations in the whole basin and different river reaches. Asterisks following slope values indicate statistically significant trends according to the M-K test ($p < 0.05$), and the dashed lines in panel (**b**) represent the corresponding Sen's trend lines.

In terms of interannual fluctuations, NDVI in the basin did not increase monotonically, but showed staged fluctuations. In the 1980s, NDVI was generally stable and increased slightly. NDVI decreased from 1990 to 1992 across all three river reaches, with more pronounced reductions in the upper and middle reaches. The 1990–1992 decline may have been associated with unfavorable hydroclimatic conditions, including reduced summer–autumn precipitation; an independent SPI- and SPEI-based assessment also identified a severe autumn drought in the upper Yangtze River Basin in 1992 [45,46]. After recovering from 1993 onward, NDVI decreased again in 2003 and recovered only partially in 2004. The relatively low NDVI value in 2004 was consistent with a documented severe autumn

drought south of the Yangtze River during August–October [47], suggesting that short-term hydroclimatic anomalies may have contributed to the interannual fluctuations in vegetation greenness [48]. NDVI subsequently entered a more pronounced increasing phase after 2005 and generally remained at relatively high levels after 2010, including during 2018–2021. Another marked decline occurred in 2022, when a compound drought–heatwave caused below-normal NDVI across the Yangtze River Basin from July to October [49]. Overall, NDVI increased significantly in the Yangtze River Basin from 1982 to 2022, but the increase differed among river sections. The middle reaches had the largest increase, the upper reaches had a weaker increase, and the lower reaches showed stronger fluctuations. This pattern may reflect the combined influence of regional climate variability and non-climatic factors, including ecological restoration and land-cover change; however, their respective contributions were not quantified in this study.

3.2.2. Spatial Variation Characteristics of Vegetation NDVI

Positive NDVI slopes occupied most of the Yangtze River Basin during 1982–2022, while local negative slopes also occurred. Significant positive slopes were distributed across large parts of the basin, especially in the middle reaches and most middle-lower reach areas, while some areas in the upper reaches also showed clear increasing trends. These patterns suggest broad vegetation improvement during the past four decades. In terms of area proportion, the NDVI-increasing area was larger than the decreasing area in all three subregions. The middle reaches showed the most prominent improvement, with FDR-significant increasing areas accounting for 59.1% and non-significantly increasing areas accounting for 20.4%, giving a total increasing area of approximately 79.5%. In the upper and lower reaches, the total increasing areas accounted for about 65.1% and 62.6%, respectively, indicating that vegetation cover improved to varying degrees in different river sections. This pattern is consistent with previous studies, which reported a basin-wide upward NDVI trend along with sustained improvement in regional ecological conditions [37]. Figure 7a displays the spatial NDVI trend classes, and Figure 7b gives their area proportions. Overall, 95.7% of the grid cells that were nominally significant remained significant after the FDR correction, confirming that the basin-wide NDVI greening pattern was robust to multiple-testing control.

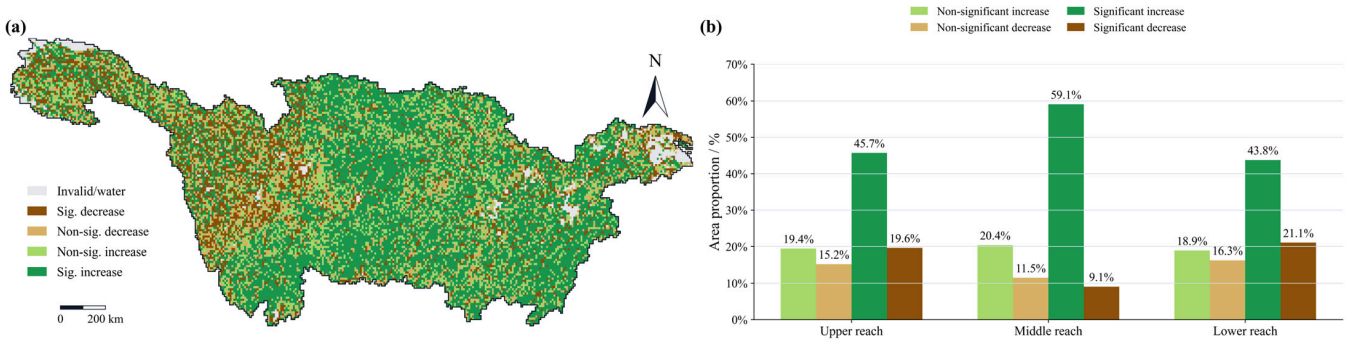


Figure 7. Spatial trends of NDVI in the Yangtze River Basin from 1982 to 2022: (**a**) spatial distribution of NDVI trends; (**b**) area proportions of different trend categories. Statistical significance was determined using Benjamini–Hochberg FDR-adjusted q values ($q < 0.05$).

At the same time, NDVI change still showed clear spatial differences. Decreasing areas were mostly distributed as scattered patches, mainly occurring in high-elevation mountainous areas of the upper reaches, mountain-transition zones, and local areas of the lower reaches. This distribution may be associated with differences in topography, regional hydrothermal variability, land-cover patterns, and the intensity of human disturbance. Compared with other subregions, the middle reaches had a higher proportion of significant

positive slopes and a lower proportion of negative slopes, indicating more stable vegetation restoration. The upper reaches have complex terrain and large elevation gradients, and some alpine grasslands and ecologically fragile areas are highly responsive to variations in water-heat conditions, making local NDVI decreases more likely. In the lower reaches, urban expansion, changes in cultivated-land use intensity, irrigation and other agricultural management practices, and fluctuations in wetland hydrological conditions may have altered local NDVI dynamics; however, their individual effects were not evaluated in this study. Overall, the spatial change in NDVI in the Yangtze River Basin can be summarized as "overall improvement, clear regional differences, and coexistence of local degradation." Among the subregions, the middle reaches showed the most significant improvement, while the upper and lower reaches showed stronger spatial heterogeneity under the background of overall improvement. The corresponding confidence intervals for the NDVI trend estimates are also reported in Table 2.

3.3. Correlations Between Extreme Climate Indices and Vegetation NDVI

The correlation matrix in Figure 8a presents NDVI–climate relationships for the basin as a whole and for individual river reaches. At basin level, temperature-based indices had stronger NDVI links than precipitation-based indices. After the FDR correction, TN90p, TX90p, and TNx remained significantly positively correlated with NDVI, whereas TN10p and TX10p remained significantly negatively correlated. TNn and TXx also had positive r values, but these relationships did not remain significant after correction. This pattern suggests that basin-scale greening during 1982–2022 was associated with fewer cold events and more warm conditions. Most precipitation-extreme indices also had positive r values with NDVI, but these relationships did not reach statistical significance. Therefore, temperature-related indices showed clearer associations with interannual NDVI fluctuations than precipitation-extreme indices at the whole-basin scale.

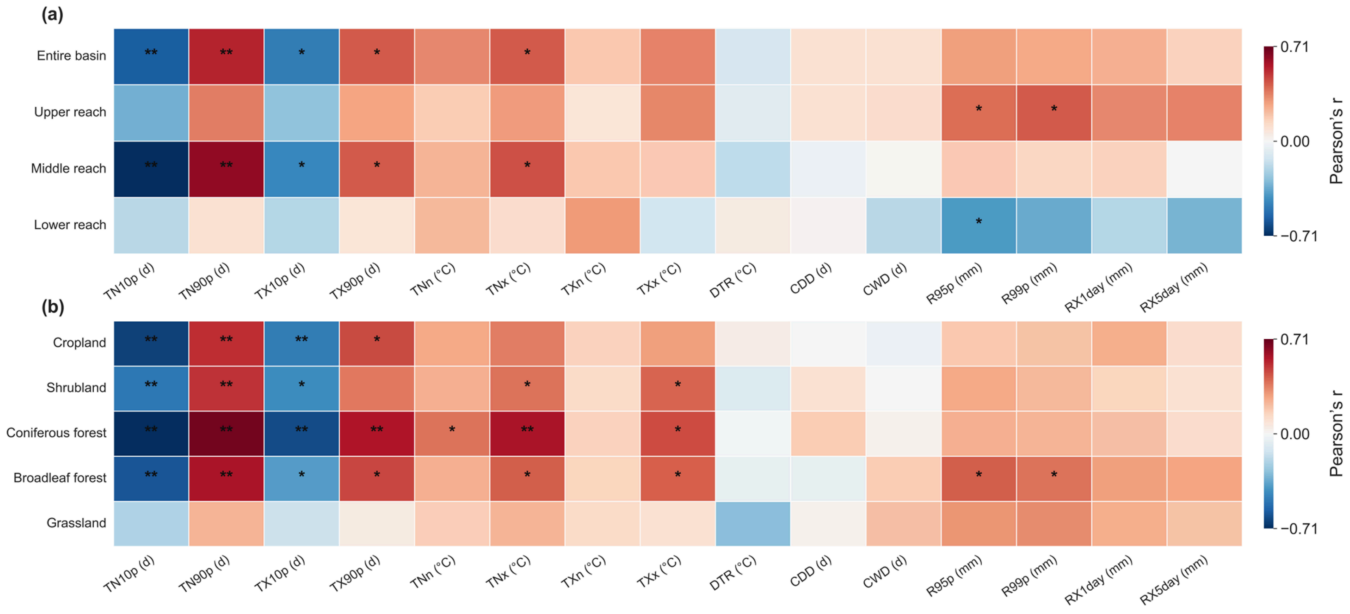


Figure 8. Correlation heatmaps showing relationships between vegetation NDVI and extreme climate indices: (**a**) different subregions; (**b**) different vegetation types. Colors represent Pearson's r. Asterisks indicate statistical significance after the Benjamini–Hochberg FDR correction: * $q < 0.05$ and ** $q < 0.01$.

The middle reaches showed the strongest temperature-related NDVI response among the three subregions. In this region, NDVI had significant positive associations with warm-related indices, including TN90p, TX90p, and TNx, and significant negative associations with TN10p and TX10p. This pattern indicates that middle-reach greening was more closely associated with thermal conditions than with precipitation extremes. In the upper reaches, NDVI was associated with both thermal and precipitation extremes. Significant positive associations remained for R95p and R99p after FDR correction, whereas RX1day and RX5day were no longer significant. The lower reaches showed different characteristics. After FDR correction, NDVI in the lower reaches remained significantly negatively correlated only with R95p; the negative correlations with R99p and RX5day were no longer significant. The retained negative association with R95p may be related to drainage conditions, flood disturbance, urbanization, and high land-use intensity in the lower-reach plains. Overall, NDVI–climate associations showed clear regional differences: temperature-related associations were strongest in the middle reaches, significant positive associations with R95p and R99p remained in the upper reaches, and a significant negative association with R95p remained in the lower reaches.

Vegetation-type responses are summarized in Figure 8b. Cultivated vegetation, shrubland, coniferous forest, and broadleaf forest shared a common temperature-response pattern: warm-related indices, including TN90p, TX90p, TNx, and TXx, corresponded to higher NDVI, whereas cold-related indices, including TN10p and TX10p, corresponded to lower NDVI. This contrast indicates that higher NDVI in these four vegetation classes was associated with warmer conditions and fewer cold extremes. Among them, coniferous forest retained the largest number of significant temperature-related associations after FDR correction, while broadleaf forest also remained significantly associated with several temperature indices.

In contrast, grassland NDVI showed relatively weak correlations with the selected climate indices, and neither R95p nor R99p remained significant after FDR correction. In addition to its significant associations with temperature indices, broadleaf forest was also positively correlated with R95p and R99p after FDR correction. Shrubland and cultivated vegetation also showed positive correlations with warm indices, but their correlations with extreme precipitation indices were relatively weak. The vegetation-type analysis revealed three main response patterns. Forests, shrubland, and cultivated vegetation were primarily associated with temperature-related indices, whereas grassland showed no significant association after FDR correction.

Pearson correlation coefficients and their 95% confidence intervals for the key annual NDVI–climate relationships discussed above are summarized in Table 3.

The partial correlation analysis showed that the number and median magnitude of significant NDVI–extreme climate relationships decreased after controlling for annual mean temperature and annual precipitation (Table 4). This reduction is expected because partial correlation analysis removes the shared variability associated with the control variables, and many extreme temperature and precipitation indices are intrinsically related to the annual thermal and moisture background. Nevertheless, several relationships remained significant after the controls, suggesting that some NDVI–extreme climate associations were relatively robust.

Table 3. Pearson correlation coefficients and 95% confidence intervals for key annual NDVI–climate relationships.

(a) Basin and Subregional Scales				
Index	**Basin**	**Upper**	**Middle**	**Lower**
TN10p	−0.59 [−0.77, −0.25]	−0.34 [−0.60, 0.05]	−0.71 [−0.84, −0.48]	−0.19 [−0.47, 0.11]
TN90p	0.54 [0.25, 0.70]	0.36 [−0.04, 0.59]	0.62 [0.39, 0.75]	0.11 [−0.27, 0.54]
TX10p	−0.49 [−0.68, −0.20]	−0.28 [−0.55, 0.09]	−0.46 [−0.61, −0.26]	−0.20 [−0.50, 0.11]
TX90p	0.43 [0.14, 0.61]	0.27 [−0.09, 0.50]	0.43 [0.11, 0.62]	0.09 [−0.24, 0.49]
TNn	0.34 [−0.01, 0.59]	0.18 [−0.22, 0.49]	0.24 [−0.10, 0.48]	0.23 [−0.13, 0.51]
TNx	0.43 [0.17, 0.63]	0.30 [−0.01, 0.51]	0.45 [0.16, 0.66]	0.12 [−0.24, 0.41]
TXn	0.19 [−0.10, 0.44]	0.09 [−0.24, 0.38]	0.18 [−0.10, 0.43]	0.30 [−0.02, 0.57]
TXx	0.35 [0.16, 0.50]	0.34 [0.10, 0.52]	0.18 [−0.11, 0.43]	−0.12 [−0.40, 0.20]
DTR	−0.11 [−0.39, 0.15]	−0.08 [−0.34, 0.16]	−0.17 [−0.46, 0.15]	0.06 [−0.21, 0.35]
CDD	0.10 [−0.26, 0.43]	0.10 [−0.22, 0.42]	−0.04 [−0.36, 0.29]	0.02 [−0.27, 0.29]
CWD	0.11 [−0.21, 0.39]	0.12 [−0.16, 0.36]	0.01 [−0.38, 0.41]	−0.18 [−0.55, 0.19]
R95p	0.29 [−0.00, 0.53]	0.40 [0.02, 0.64]	0.18 [−0.07, 0.41]	−0.40 [−0.63, −0.12]
R99p	0.27 [−0.02, 0.49]	0.43 [0.04, 0.64]	0.15 [−0.12, 0.41]	−0.35 [−0.62, 0.02]
RX1day	0.24 [−0.04, 0.45]	0.33 [0.02, 0.56]	0.16 [−0.13, 0.42]	−0.20 [−0.53, 0.17]
RX5day	0.16 [−0.20, 0.45]	0.34 [−0.05, 0.59]	−0.01 [−0.29, 0.27]	−0.33 [−0.60, 0.03]

(b) Vegetation-Type Scale					
Index	**Cultivated Vegetation**	**Shrubland**	**Coniferous Forest**	**Broadleaf Forest**	**Grassland**
TN10p	−0.66 [−0.79, −0.45]	−0.51 [−0.74, −0.10]	−0.71 [−0.85, −0.43]	−0.60 [−0.78, −0.26]	−0.21 [−0.48, 0.16]
TN90p	0.52 [0.30, 0.69]	0.51 [0.12, 0.71]	0.68 [0.37, 0.80]	0.57 [0.24, 0.73]	0.24 [−0.13, 0.47]
TX10p	−0.49 [−0.62, −0.31]	−0.44 [−0.69, −0.09]	−0.63 [−0.77, −0.38]	−0.39 [−0.61, −0.09]	−0.15 [−0.44, 0.19]
TX90p	0.46 [0.21, 0.68]	0.37 [0.03, 0.58]	0.57 [0.29, 0.70]	0.47 [0.13, 0.65]	0.06 [−0.28, 0.32]
TNn	0.27 [−0.12, 0.53]	0.25 [−0.05, 0.50]	0.38 [0.09, 0.59]	0.25 [−0.09, 0.52]	0.17 [−0.17, 0.49]
TNx	0.36 [0.10, 0.61]	0.38 [0.12, 0.57]	0.57 [0.33, 0.72]	0.42 [0.19, 0.59]	0.24 [−0.07, 0.47]
TXn	0.16 [−0.06, 0.38]	0.13 [−0.15, 0.37]	0.16 [−0.12, 0.38]	0.15 [−0.15, 0.38]	0.13 [−0.19, 0.45]
TXx	0.29 [0.04, 0.51]	0.41 [0.22, 0.54]	0.46 [0.26, 0.62]	0.42 [0.17, 0.55]	0.10 [−0.16, 0.33]
DTR	0.05 [−0.23, 0.31]	−0.09 [−0.37, 0.14]	−0.02 [−0.33, 0.25]	−0.05 [−0.31, 0.16]	−0.29 [−0.47, −0.06]
CDD	−0.01 [−0.29, 0.29]	0.10 [−0.26, 0.45]	0.18 [−0.25, 0.51]	−0.05 [−0.32, 0.19]	0.03 [−0.29, 0.37]
CWD	−0.03 [−0.44, 0.39]	−0.01 [−0.27, 0.23]	0.03 [−0.24, 0.33]	0.17 [−0.20, 0.45]	0.21 [−0.10, 0.46]
R95p	0.19 [−0.08, 0.43]	0.27 [−0.03, 0.49]	0.25 [−0.04, 0.49]	0.42 [0.09, 0.69]	0.31 [−0.00, 0.56]
R99p	0.20 [−0.06, 0.45]	0.23 [−0.07, 0.45]	0.24 [−0.03, 0.47]	0.39 [0.02, 0.66]	0.33 [0.04, 0.55]
RX1day	0.26 [−0.00, 0.48]	0.15 [−0.12, 0.37]	0.21 [−0.04, 0.43]	0.29 [−0.03, 0.55]	0.26 [−0.07, 0.49]
RX5day	0.12 [−0.23, 0.42]	0.10 [−0.21, 0.38]	0.12 [−0.15, 0.38]	0.28 [−0.09, 0.58]	0.20 [−0.09, 0.46]

Note: Values are Pearson's correlation coefficients, with 95% confidence intervals in brackets. Confidence intervals were estimated using a three-year moving block bootstrap. Only key correlations discussed in the text are listed. Statistical significance after the Benjamini–Hochberg false discovery rate correction is indicated in Figure 8.

Table 4. Summary of partial correlation analysis after controlling for annual mean temperature and annual precipitation.

Panel	Total Relationships	Pearson $p < 0.05$	Partial $p < 0.05$	Median |Pearson r|	Median |Partial r|
Basin/subregions	60	22	5	0.231	0.124
Vegetation types	75	28	7	0.254	0.117
Overall	135	50	12	0.244	0.117

Note: Partial correlations were calculated after controlling for annual mean temperature and annual precipitation. Counts indicate nominally significant relationships at $p < 0.05$.

3.4. Lagged Cumulative Effects of Extreme Climate Indices on Vegetation NDVI

To further characterize the temporal response of vegetation to extreme climate conditions, the lagged cumulative analysis was conducted to account for the possibility that vegetation responses may extend beyond the month in which a climate extreme occurs. The analysis evaluates the associations between NDVI and extreme climate indices over different response windows, thereby providing a basis for examining temporal differences in vegetation responses among subregions and vegetation types. The FDR-adjusted significance statistics are summarized in Table 5. The correction did not change the selected optimal LA windows, but it reduced the proportion of significant pixels for several cold-

and warm-event frequency indices, indicating that these associations should be interpreted more cautiously.

Table 5. FDR-adjusted significance results for the lag–accumulation analysis.

Index	Tested Windows	Pixel Original $p < 0.05$	Pixel FDR q < 0.05	Pixel Change (pp)	Interpretation
DTR	10	99.65%	98.92%	−0.73	Stable
RX1day	10	99.97%	99.89%	−0.08	Stable
RX5day	10	99.99%	99.94%	−0.05	Stable
TN10p	10	48.57%	34.99%	−13.58	More conservative
TN90p	10	61.00%	45.19%	−15.81	More conservative
TNn	10	99.99%	99.96%	−0.03	Stable
TNx	10	99.98%	99.94%	−0.04	Stable
TX10p	10	47.39%	30.87%	−16.53	More conservative
TX90p	10	49.44%	34.54%	−14.9	More conservative
TXn	10	99.97%	99.95%	−0.03	Stable
TXx	10	99.90%	99.79%	−0.11	Stable

Note: FDR, false discovery rate; LA, lag–accumulation. FDR correction was applied across the ten candidate LA windows tested for each NDVI–climate pair. "Pixel original $p < 0.05$" indicates the proportion of pixels significant before correction, whereas "Pixel FDR q < 0.05" indicates the proportion remaining significant after Benjamini–Hochberg correction.

3.4.1. Lagged Cumulative Effects of Extreme Climate Indices on Vegetation NDVI Among Subregions

Pixel-level optimal lag-accumulation (LA) types were mapped to examine how NDVI responded to extreme climate indices across the Yangtze River Basin (Figures 9 and 10). The resulting maps show marked spatial variation in NDVI–climate response windows. For most indices, pure cumulative responses occupied the largest area, meaning that NDVI was linked not only to climate conditions in the current month but also to climate conditions accumulated from previous months. In terms of the area proportion across the whole basin, the proportions of pure cumulative responses for RX1day, RX5day, TN90p, TNn, TNx, TXn, and TXx all exceeded 70%. For temperature-intensity indices, including TNn, TNx, TXn, and TXx, this response type covered 86.4–88.8% of the basin, showing that their NDVI relationships were largely controlled by short-term accumulation. The pure cumulative response proportions of RX1day and RX5day were 74.5% and 77.6%, respectively, indicating that the relationships between heavy precipitation indices and NDVI also showed clear cumulative effects.

The LA types differed among regions and indices. For RX1day and RX5day (Figure 9b,c), L0A2 occupied most of the upper reaches, indicating that NDVI in these areas was most strongly associated with heavy precipitation accumulated over the current month and the preceding two months. In the middle and lower reaches, especially across the Jianghan lowland, the Dongting-Poyang lake area, and downstream plain regions, lagged cumulative types such as L1A2 and L2A1 increased markedly. These spatial differences indicate that the timing of the strongest precipitation–NDVI associations varied among the upper, middle, and lower reaches. In contrast, DTR (Figure 9a) showed the strongest spatial heterogeneity. Lagged cumulative responses were common in the Sichuan lowland and parts of the middle-reach region, whereas short-term cumulative responses appeared more frequently in the western part of the upper reach and in localized downstream areas. These results show that the optimal association windows between DTR and NDVI varied considerably across different terrain and hydrothermal regions.

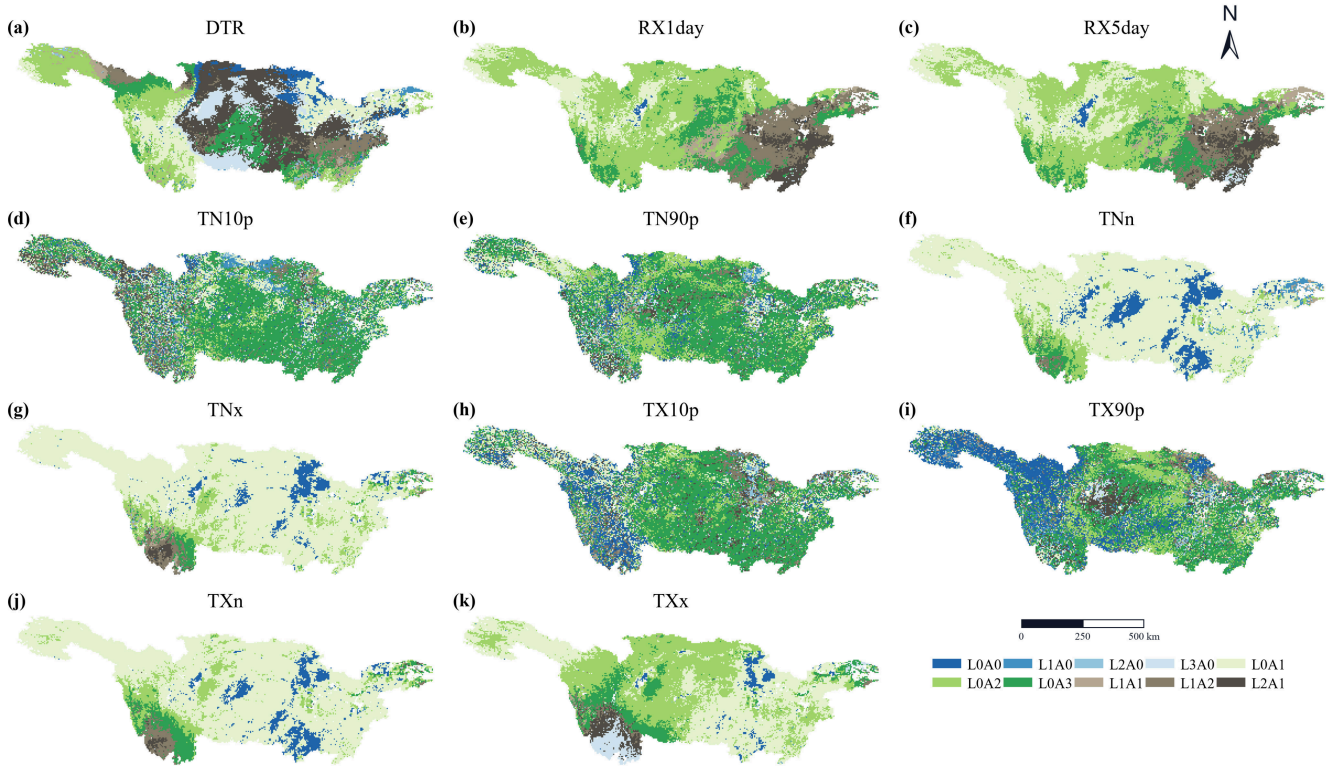


Figure 9. Spatial distribution of optimal lag-accumulation response types between NDVI and extreme climate indices in the Yangtze River Basin. In the notation used in this study, Lx indicates a starting lag of x months, whereas Ay indicates y additional preceding months; therefore, each window spans offsets x through x + y and contains y + 1 monthly climate values. For example, L0A0 includes only the current month, L0A2 includes the current month and the preceding two months, and L1A2 includes the preceding one to three months. Abbreviations and definitions of the extreme climate indices are provided in Table 1.

The spatial patterns of temperature indices can be separated into cold/warm event frequency indices and temperature-intensity indices. For TN10p and TX10p (Figure 9d,h), L0A3 dominated most areas of the middle and lower reaches, accounting for 47.2% and 44.2%, respectively. This indicates that cold events had relatively obvious multi-month cumulative effects on vegetation NDVI. However, in high-elevation areas and mountain-transition zones of the upper reaches, response types were more fragmented. This pattern is likely related to elevation, topography, and low-temperature limitation, which together produce more complex vegetation-response processes. Warm-event frequency indices TN90p and TX90p (Figure 9e,i) also showed cumulative responses in the middle and lower reaches. However, TX90p showed more current-month or short-lag responses in the western upper reaches, suggesting that high-temperature effects were likely constrained by both water availability and thermal limitation.

Temperature-intensity indices, including TXn, TXx, TNn and TNx (Figure 9f,g,j,k) displayed the most continuous spatial patterns. TNn, TNx, and TXn were mainly associated with L0A1 across most of the basin, with area proportions of 74.5%, 75.0%, and 72.3%, respectively. Their effects on NDVI therefore occurred mainly within the current month and a short preceding window. TXx was jointly dominated by L0A1 and L0A2, with area proportions of 39.9% and 38.3%, respectively, indicating that extreme maximum temperature affected vegetation both immediately and cumulatively. Spatially, the middle-lower reach plains and hilly areas were dominated by short-term cumulative responses, showing relatively continuous patterns. In contrast, lagged cumulative or lagged response patches appeared for several temperature indices in the southwestern mountain-

ous and high-elevation areas of the upper reaches, indicating that vegetation responses to extreme temperature in complex terrain areas are more easily regulated by antecedent hydrothermal conditions.

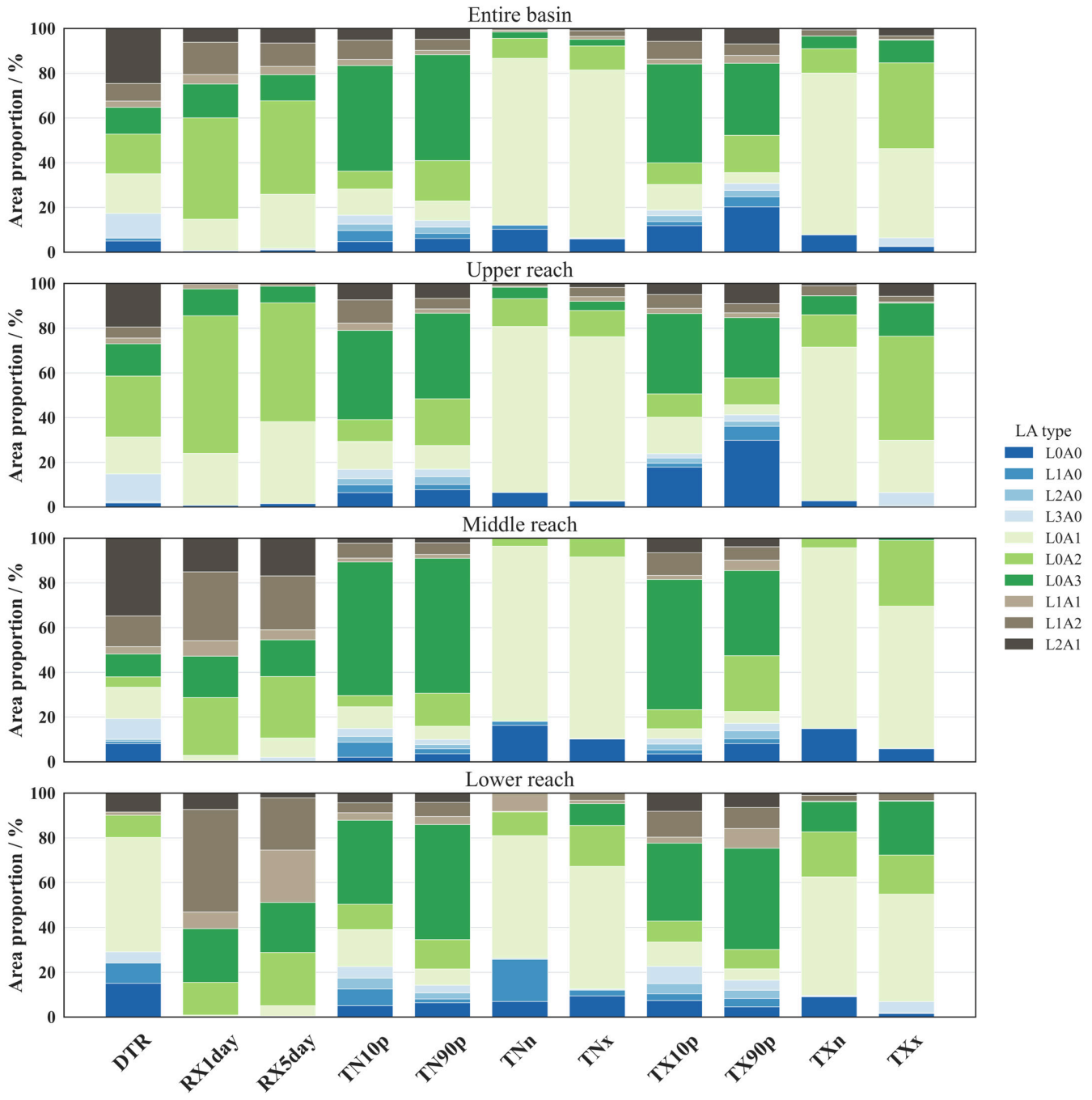


Figure 10. Area proportions of optimal lag-accumulation response types between NDVI and extreme climate indices in different river reaches of the Yangtze River Basin. In the notation used in this study, Lx indicates a starting lag of x months, whereas Ay indicates y additional preceding months; therefore, each window spans offsets x through x + y and contains y + 1 monthly climate values. Abbreviations and definitions of the extreme climate indices are provided in Table 1.

The subregional area proportions of these optimal LA response types are summarized in Figure 10, which further confirms the dominance of cumulative responses and the regional contrasts across the three river sections. At the basin scale, the lagged cumulative effects of extreme climate indices on NDVI can be described as follows: short-term cumu-

lative responses were spatially continuous in the middle and lower reaches; upper-reach mountainous areas had more complex response types; and precipitation indices showed stronger lagged effects across the middle-lower basin. Temperature-intensity extremes mainly affected vegetation NDVI through short-term cumulative processes, whereas the effects of extreme precipitation and DTR showed stronger regional differences and lagged transmission characteristics. This reflects the joint role of topography, soil moisture conditions, hydrological processes, and vegetation types in shaping temporal variability in NDVI responses to climate extremes across the basin.

3.4.2. Lagged Cumulative Effects of Extreme Climate Indices on NDVI Among Different Vegetation Types

Figure 11 shows that the optimal LA types of NDVI–climate associations differed among vegetation types, although cumulative windows were dominant overall. Temperature indices were dominated by pure cumulative responses across all vegetation types, indicating that NDVI responses to temperature change were more often reflected by the continuous effects of current and antecedent temperature conditions. Among the vegetation types, broadleaf forest had the highest proportion of pure cumulative responses to temperature indices, at 84.8%; the corresponding proportions for shrubland, coniferous forest, grassland, and cultivated vegetation were 79.4%, 77.7%, 75.6%, and 73.1%, respectively. For specific indices, TNn, TNx, and TXn were mostly dominated by L0A1, whereas TN10p, TN90p, TX10p, and TX90p more often showed L0A3, indicating that the response windows of extreme temperature intensity indices were relatively short, while cold- and warm-event frequency indices showed more obvious multi-month cumulative characteristics.

Extreme precipitation indices also mainly showed cumulative responses among different vegetation types, but the response intensity varied. Grassland and shrubland had relatively high proportions of pure cumulative responses to RX1day and RX5day, at 88.5% and 87.0%, respectively; the proportion for broadleaf forest was 81.2%, while those for cultivated vegetation and coniferous forest were 65.4% and 68.2%, respectively. Meanwhile, cultivated vegetation and coniferous forest had relatively high proportions of lagged cumulative responses, at 32.3% and 30.8%, respectively, indicating that these two vegetation types showed certain delayed responses to extreme precipitation. In terms of LA types, RX1day and RX5day were dominated by L0A2 in most vegetation types, indicating that the effects of heavy precipitation on NDVI were mainly concentrated within the current month and the short antecedent accumulation window.

The response types of DTR differed more noticeably among vegetation types. The proportions of lagged cumulative responses to DTR were 48.5%, 38.4%, 35.4%, and 34.6% for broadleaf forest, cultivated vegetation, shrubland, and coniferous forest, respectively. In contrast, grassland was dominated by pure cumulative responses, accounting for 66.2%, among which L0A2 had the highest proportion, at 39.5%. Taken together, the vegetation-type results reveal three main LA-response patterns: temperature indices were generally dominated by pure cumulative responses; extreme precipitation indices were dominated by short-term cumulative responses, although some vegetation types showed lagged cumulative characteristics; and DTR showed the most pronounced differences among vegetation types.

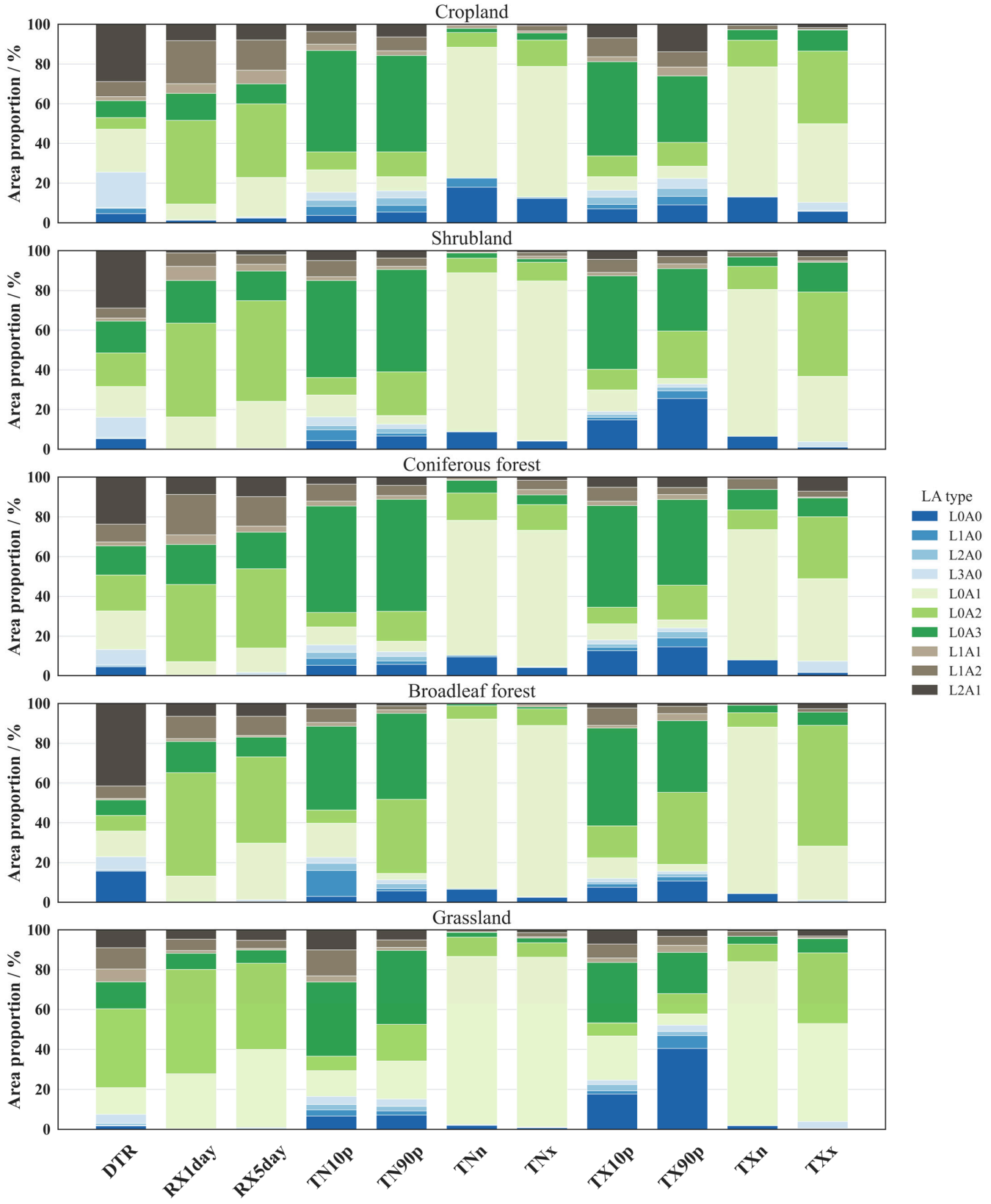


Figure 11. Area proportions of optimal lag-accumulation response types between NDVI and extreme climate indices among different vegetation types. In the notation used in this study, Lx indicates a starting lag of x months, whereas Ay indicates y additional preceding months; therefore, each window spans offsets x through x + y and contains y + 1 monthly climate values. Abbreviations and definitions of the extreme climate indices are provided in Table 1.

4. Discussion

4.1. Vegetation Trends, Climate Associations, and Ecological Interpretations

A basin-scale increase in NDVI was detected across the Yangtze River Basin during 1982–2022, indicating an overall improvement in vegetation cover. This pattern agrees with earlier reports showing a general NDVI increase across the basin and the dominance of areas with positive NDVI trends [37]. However, from the perspective of spatial patterns, vegetation improvement did not occur uniformly. The middle reaches showed the most significant improvement, while the upper and lower reaches also increased overall but had relatively concentrated local decreasing areas. These spatial contrasts suggest that topography, background climate, and anthropogenic activities jointly shaped vegetation dynamics in the basin [50]. Multiple-testing control revealed a clear contrast among the spatial trend results. Most temperature-extreme and NDVI trends remained significant after the FDR correction, whereas none of the grid-cell-level precipitation-extreme trends did. Similar losses of field significance have been reported for relatively short and highly variable extreme-precipitation records, indicating that the precipitation slope maps should be interpreted as spatial tendencies rather than definitive local changes [51].

The correlation results indicate a more stable NDVI response to temperature-related indices. Overall, warm-related indices and temperature-intensity indices generally corresponded to higher NDVI, whereas cold-related indices corresponded to lower NDVI. This association is consistent with the reported sensitivity of vegetation greenness to thermal conditions across the Yangtze River Basin. Similar temperature sensitivity has been reported for vegetation across the Yangtze River Basin and eastern China [19]. By comparison, the NDVI response to extreme precipitation showed greater spatial variation. Some areas in the upper reaches showed positive responses, whereas local areas in the lower reaches showed negative responses. Possible explanations for these contrasting associations include differences in water availability, waterlogging, surface runoff, and local drainage conditions; however, these processes were not directly evaluated in this study [25].

The contrasting climate associations among vegetation types may reflect differences in physiological and environmental constraints. The comparatively strong associations of coniferous and broadleaf forest NDVI with temperature-related indices are consistent with the role of temperature in regulating canopy activity, phenological transitions, and the duration of the photosynthetically active season [52]. Warmer conditions and fewer cold extremes may therefore prolong the period suitable for forest canopy activity, providing a plausible explanation for the stronger temperature associations of forest vegetation. By contrast, grassland NDVI showed relatively weak associations with the selected extreme climate indices, and none remained significant after FDR correction. This contrast suggests that grassland greenness may be influenced by multiple interacting constraints, including water availability and non-climatic disturbances, rather than by a dominant association with any single extreme climate index. Biome-scale research has similarly shown that vegetation sensitivity to water deficits varies among ecosystem types and drought time scales [24]. Broadleaf forest was associated with both temperature and heavy-precipitation indices, indicating that soil-moisture replenishment may operate alongside temperature-related controls. The response of cultivated vegetation may additionally be modified by planting schedules, irrigation, and other agricultural practices. Because these physiological and management processes were not directly measured, they should be regarded as plausible ecological explanations rather than mechanisms demonstrated by the present analysis.

The lagged cumulative analysis further showed that NDVI–climate associations were not limited to the current month, but were more often stronger when current and antecedent climate conditions were considered together. Temperature indices were generally dominated by cumulative windows, indicating that multi-month temperature conditions

were more strongly associated with NDVI than single-month conditions in many areas. The effects of precipitation were more likely to show a certain lag, which is consistent with the understanding that NDVI responses to precipitation usually have longer lag times than responses to temperature [21]. Considering lagged and cumulative windows can therefore provide a more complete characterization of the temporal associations between climate anomalies and vegetation NDVI [30].

The LA results for different vegetation types showed that all vegetation types generally exhibited cumulative responses to temperature indices, but their responses to extreme precipitation and DTR differed more clearly. In this study, grassland, shrubland, and broadleaf forest mostly showed short-term cumulative responses to extreme precipitation, whereas cultivated vegetation and coniferous forest had relatively higher proportions of lagged cumulative responses. This indicates that vegetation types differed in the timing of their responses to climatic drivers. Earlier studies have also shown that the correlations and lag periods between NDVI and temperature or precipitation differ among vegetation-cover types, and results at the basin-average scale may mask response differences among vegetation types [23].

4.2. Limitations and Future Perspectives

Although the integration of long-term meteorological and NDVI records provides a consistent basis for examining climate–vegetation relationships across the Yangtze River Basin, the scope and resolution of the conclusions are constrained by the statistical design, input datasets, spatial classification, and explanatory variables considered. These limitations are discussed below to clarify the appropriate interpretation and application of the results.

First, this study was designed to identify statistical relationships rather than establish causal effects. The partial correlation analysis showed that many NDVI–extreme climate correlations weakened after controlling for annual mean temperature and annual precipitation, indicating that these relationships were partly embedded in the broader hydrothermal background. This does not invalidate the original Pearson correlations, but suggests that they should be interpreted as climate-related statistical associations rather than independent causal effects of individual extreme climate indices, consistent with evidence that vegetation dynamics are jointly regulated by climatic, ecological, and anthropogenic drivers [11,53]. Similarly, the optimal lag–accumulation (LA) window represents the period over which an extreme climate index showed the strongest association with NDVI after antecedent months were incorporated; it does not demonstrate that the climatic event caused the subsequent vegetation change. Establishing causal relationships would require additional controls for covarying climatic conditions and non-climatic drivers.

Second, uncertainty also arises from the spatial datasets used in the analysis. CN05.1 was generated by interpolating meteorological-station observations, and previous evaluations over the Tibetan Plateau have shown that sparse station coverage and complex terrain can increase uncertainty in the spatial representation of temperature and precipitation [38,54,55]. This issue is particularly relevant to the high-elevation upper Yangtze River Basin. We therefore place greater interpretive emphasis on basin- and subregion-scale patterns than on differences among individual grid cells in this area. PKU-GIMMS NDVI V1.2 provides a harmonized long-term record reconstructed from GIMMS NDVI3g using Landsat reference samples and subsequently consolidated with MODIS NDVI [12]. Although the product has been validated against independent Landsat samples and showed strong agreement with MODIS NDVI during the overlapping period, its developers identified remaining uncertainties associated with Landsat sample errors and uneven sample availability, the biome-specific neural-network reconstruction, the static

land-cover information used in product development, and uncertainties inherited from GIMMS NDVI3g [12]. Because only PKU-GIMMS NDVI V1.2 was used in the present study, the sensitivity of the detected trends and climate–NDVI associations to the choice of NDVI product was not independently evaluated. In addition, NDVI saturation may reduce sensitivity to subtle vegetation changes in densely vegetated areas [56]. Therefore, local trend magnitudes and differences among densely vegetated regions should be interpreted cautiously, and future studies should conduct cross-product comparisons over overlapping periods.

Third, the vegetation-type comparison is subject to uncertainty arising from the conversion of the static vegetation map to the 1/12° analysis grid. Nearest-neighbor resampling preserved the original categorical information, but each target grid cell was assigned a single vegetation class. Mixed pixels and vegetation-transition zones may therefore not be fully represented, and vegetation-type differences near class boundaries should be interpreted cautiously. In addition, previous studies have documented extensive ecological restoration and afforestation within the Yangtze River Basin, together with urban and construction-land expansion in rapidly developing areas [18,50,57]. The static vegetation map used in this study served only to group pixels by vegetation type and could not characterize interannual land-use and land-cover changes. Annual land-cover, irrigation, and agricultural-management data were not included in the present analysis; therefore, the individual contributions of urbanization, afforestation, ecological restoration, irrigation, and agricultural management to NDVI variations during 1982–2022 could not be quantified. These unmeasured human-related factors may confound the interpretation of both the detected NDVI trends and the estimated climate–NDVI associations. The correlation and LA results should therefore be interpreted as statistical associations with extreme climate indices rather than as estimates of the climatic contribution to vegetation greening. CO_2 fertilization may also have contributed to long-term vegetation greening but was not evaluated separately in this study [14]. Future research incorporating temporally consistent land-cover, irrigation, ecological-restoration, agricultural-management, and atmospheric CO_2 data would be required to distinguish climatic from non-climatic contributions.

Finally, the ETCCDI-based index set used in this study represents warm and wet extremes more comprehensively than drought-related processes. Within this framework, drought-related information is mainly characterized by CDD, which records the longest sequence of days with daily precipitation below 1 mm [3]. Therefore, conclusions concerning water limitation in this study are restricted to precipitation persistence and do not represent cumulative water deficits, atmospheric evaporative demand, or soil-moisture drought. Future work should combine multiscalar meteorological drought indicators and soil-moisture observations with time-varying non-climatic drivers such as land-cover change, irrigation, ecological restoration, agricultural management, and atmospheric CO_2. It should also compare multiple vegetation products and test non-standard percentile thresholds, such as the 5th/95th percentiles, where rarer extremes are of interest; a multivariable attribution framework would further help distinguish climatic from non-climatic contributions.

5. Conclusions

(1) During 1982–2022, the Yangtze River Basin experienced a basin-wide rise in NDVI, pointing to an overall improvement in vegetation cover. Spatially, positive NDVI slopes occupied most of the basin, and the middle reaches showed the clearest greening signal. The upper and lower reaches also had predominantly positive NDVI slopes, but local negative-slope patches were more evident, implying stronger spatial unevenness.

(2) NDVI had clear relationships with extreme temperature indices. Warm-related indices and temperature-intensity indices corresponded to higher NDVI, whereas cold-related indices corresponded to lower NDVI, indicating that vegetation greenness was associated with warmer conditions and fewer cold extremes. NDVI–precipitation relationships varied among regions: upper-reach areas tended to show positive associations, whereas several lower-reach areas showed negative associations.

(3) The LA analysis indicated that the strongest associations between NDVI and extreme climate in the Yangtze River Basin were mainly identified within cumulative windows. Temperature indices mainly showed short-term or multi-month cumulative association windows, while extreme precipitation indices showed lagged cumulative characteristics in some regions, indicating that antecedent climate conditions provided additional information beyond current-month conditions.

(4) NDVI–extreme-climate associations differed among vegetation types. Temperature indices were dominated by cumulative association windows across all vegetation types. The association strength and lag characteristics of extreme precipitation indices differed among vegetation types, and DTR showed the most pronounced differences among LA types. These results indicate that NDVI–extreme-climate association patterns vary by both river reach and vegetation type.

Author Contributions: Conceptualization, X.C., Y.M. and X.D.; methodology, X.C.; software, X.C.; validation, X.C.; formal analysis, X.C.; investigation, X.C.; resources, X.D. and Y.M.; data curation, X.C.; writing—original draft preparation, X.C.; writing—review and editing, X.C., Y.M., X.D., Q.Y. and C.G.; visualization, X.C.; supervision, Y.M.; project administration, Y.M. and X.D.; funding acquisition, Y.M. All authors have read and agreed to the published version of the manuscript.

Funding: This research was funded by the National Natural Science Foundation of China [grant number U2442213].

Data Availability Statement: The CN05.1 daily gridded meteorological dataset can be obtained from the website https://nzc.iap.ac.cn/content?aid=999&cid=24, accessed on 11 March 2026. The PKU-GIMMS NDVI V1.2 dataset can be obtained from the website https://zenodo.org/records/8253971, accessed on 11 March 2026. The vegetation-type data can be obtained from the National Cryosphere Desert Data Center website https://www.ncdc.ac.cn/, accessed on 11 March 2026.

Conflicts of Interest: The authors declare no conflicts of interest.

References

1. IPCC. *Climate Change 2021: The Physical Science Basis*; Cambridge University Press: Cambridge, UK, 2021. [CrossRef]
2. David, E.; Gerald, A.M.; Camille, P.; Stanley, A.C. Climate extremes: Observations, modeling, and impacts. *Science* **2000**, *289*, 2068–2074. [CrossRef] [PubMed]
3. Zhang, X.B.; Alexander, L.; Hegerl, G.C.; Jones, P.; Tank, A.K.; Peterson, T.C.; Trewin, B.; Zwiers, F.W. Indices for monitoring changes in extremes based on daily temperature and precipitation data. *Wiley Interdiscip. Rev. Clim. Change* **2011**, *2*, 851–870. [CrossRef]
4. Donat, M.G.; Alexander, L.V.; Yang, H.; Durre, I.; Vose, R.; Dunn, R.J.H.; Willett, K.M.; Aguilar, E.; Brunet, M.; Caesar, J.; et al. Updated analyses of temperature and precipitation extreme indices since the beginning of the twentieth century: The HadEX2 dataset. *J. Geophys. Res. Atmos.* **2013**, *118*, 2098–2118. [CrossRef]
5. You, Q.; Kang, S.; Aguilar, E.; Pepin, N.; Fluegel, W.-A.; Yan, Y.; Xu, Y.; Zhang, Y.; Huang, J. Changes in daily climate extremes in China and their connection to the large scale atmospheric circulation during 1961–2003. *Clim. Dyn.* **2011**, *36*, 2399–2417. [CrossRef]
6. Yin, H.; Sun, Y. Analysis of extreme temperature and precipitation characteristics in China in 2017 based on ETCCDI indices. *Clim. Change Res.* **2019**, *15*, 363–373. [CrossRef]
7. Qian, Z.H.; Sun, Y.X.; Ma, Q.R.; Gu, Y.; Feng, T.C.; Feng, G.L. Understanding changes in heat waves, droughts, and compound events in Yangtze River Valley and the corresponding atmospheric circulation patterns. *Clim. Dyn.* **2024**, *62*, 539–553. [CrossRef]

8. Sun, H.H.; Zhang, X.P.; Luo, Z.D.; Shang, C.P.; He, X.G.; Rao, Z.G. Characteristics of extreme precipitation indices in the Yangtze River Basin over the past 53 years. *Resour. Environ. Yangtze Basin* **2018**, *27*, 1879–1890.
9. Wang, Q.; Zhang, M.J.; Wang, S.J.; Lu, S.F.; Wang, B.L.; Zhu, X.F. Analysis of extreme temperature events in the Yangtze River Basin from 1962 to 2011. *Acta Geogr. Sin.* **2013**, *68*, 611–625. [CrossRef]
10. Tucker, C.J. Red and photographic infrared linear combinations for monitoring vegetation. *Remote Sens. Environ.* **1979**, *8*, 127–150. [CrossRef]
11. Zeng, Y.L.; Hao, D.L.; Huete, A.; Dechant, B.; Berry, J.; Chen, J.M.; Joiner, J.; Frankenberg, C.; Bond-Lamberty, B.; Ryu, Y.; et al. Optical vegetation indices for monitoring terrestrial ecosystems globally. *Nat. Rev. Earth Environ.* **2022**, *3*, 477–493. [CrossRef]
12. Gustau, C.V.; Manuel, C.T.; Alvaro, M.M.; Sophia, W.; Gregory, D.; Alessandro, C.; Mahecha, M.D.; Munoz-Mari, J. A unified vegetation index for quantifying the terrestrial biosphere. *Sci. Adv.* **2021**, *7*, eabc7447. [CrossRef] [PubMed]
13. Li, M.Y.; Cao, S.; Zhu, Z.C.; Wang, Z.; Myneni, R.B.; Piao, S.L. Spatiotemporally consistent global dataset of the GIMMS Normalized Difference Vegetation Index (PKUGIMMSNDVI) from 1982 to 2022. *Earth Syst. Sci. Data* **2023**, *15*, 4181–4203. [CrossRef]
14. Fensholt, R.; Proud, S.R. Evaluation of Earth Observation based global long term vegetation trends—Comparing GIMMS and MODIS global NDVI time series. *Remote Sens. Environ.* **2012**, *119*, 131–147. [CrossRef]
15. Zhu, Z.C.; Piao, S.L.; Myneni, R.B.; Huang, M.T.; Zeng, Z.Z.; Canadell, J.G.; Ciais, P.; Sitch, S.; Friedlingstein, P.; Arneth, A.; et al. Greening of the Earth and its drivers. *Nat. Clim. Change* **2016**, *6*, 791–795. [CrossRef]
16. Piao, S.L.; Yin, G.D.; Tan, J.G.; Cheng, L.; Huang, M.T.; Li, Y.; Liu, R.G.; Mao, J.; Myneni, R.B.; Peng, S.; et al. Detection and attribution of vegetation greening trend in China over the last 30 years. *Glob. Change Biol.* **2015**, *21*, 1601–1609. [CrossRef] [PubMed]
17. Gao, J.B.; Jiao, K.W.; Wu, S.H. Climatic influence analysis of the spatial heterogeneity of vegetation NDVI in China from 1982 to 2013. *Acta Geogr. Sin.* **2019**, *74*, 534–543. [CrossRef]
18. Zhang, L.; Ding, M.; Zhang, H.; Wen, C. Spatiotemporal changes in vegetation coverage in the Yangtze River Basin from 1982 to 2015. *J. Nat. Resour.* **2018**, *33*, 2084–2097. [CrossRef]
19. Qu, S.; Wang, L.C.; Lin, A.W.; Zhu, H.J.; Yuan, M.X. What drives the vegetation restoration in Yangtze River basin, China: Climate change or anthropogenic factors? *Ecol. Indic.* **2018**, *90*, 438–450. [CrossRef]
20. Wang, Q.; Ju, Q.; Wang, Y.Y.; Fu, X.L.; Zhao, W.J.; Du, Y.H.; Jiang, P.; Hao, Z.C. Regional patterns of vegetation dynamics and their sensitivity to climate variability in the Yangtze River Basin. *Remote Sens.* **2022**, *14*, 5623. [CrossRef]
21. Zhang, M.Y.; Wang, K.L.; Liu, H.Y.; Yue, Y.M.; Ren, Y.J.; Chen, Y. Vegetation inter-annual variation responses to climate variation in different geomorphic zones of the Yangtze River Basin, China. *Ecol. Indic.* **2023**, *152*, 110357. [CrossRef]
22. Cui, L.L.; Shi, J.; Yang, Y.M.; Fan, Y.W. Response characteristics of vegetation NDVI to temperature and precipitation at ten-day scale in eastern China. *Acta Geogr. Sin.* **2009**, *64*, 850–860. [CrossRef]
23. Chen, Z.F.; Wang, W.G.; Fu, J.Y. Vegetation response to precipitation anomalies under different climatic and biogeographical conditions in China. *Sci. Rep.* **2020**, *10*, 830. [CrossRef] [PubMed]
24. Lu, Q.Q.; Jiang, T.; Liu, D.L.; Liu, Z.Y. Response characteristics of NDVI of different vegetation cover types in China to temperature and precipitation. *Ecol. Environ. Sci.* **2020**, *29*, 23–34. [CrossRef]
25. Vicente Serrano, S.M.; Gouveia, C.; Camarero, J.J.; Begueria, S.; Trigo, R.; Lopez Moreno, J.I.; Azorin Molina, C.; Pasho, E.; Lorenzo Lacruz, J.; Revuelto, J.; et al. Response of vegetation to drought time-scales across global land biomes. *Proc. Natl. Acad. Sci. USA* **2013**, *110*, 52–57. [CrossRef] [PubMed]
26. Jin, J.X.; Xiao, Y.Y.; Jin, J.L.; Zhu, Q.W.; Yong, B.; Ji, Y. Spatiotemporal variation characteristics of extreme hydrometeorological events in the Yangtze River Basin and their effects on vegetation. *Adv. Water Sci.* **2021**, *32*, 867–876. [CrossRef]
27. Ni, M.; Zhang, X.Y.; Jiang, C.; Wang, H.S. Responses of vegetation to extreme climate events in southwestern China. *Chin. J. Plant Ecol.* **2021**, *45*, 626–640. [CrossRef]
28. Ji, L.; Peters, A.J. Lag and seasonality considerations in evaluating AVHRR NDVI response to precipitation. *Photogramm. Eng. Remote Sens.* **2005**, *71*, 1053–1061. [CrossRef]
29. Ogle, K.; Barber, J.J.; Barron-Gafford, G.A.; Bentley, L.P.; Young, J.M.; Huxman, T.E.; Loik, M.E. Quantifying ecological memory in plant and ecosystem processes. *Ecol. Lett.* **2015**, *18*, 221–235. [CrossRef] [PubMed]
30. Ding, Y.X.; Li, Z.; Peng, S.Z. Global analysis of time-lag and -accumulation effects of climate on vegetation growth. *Int. J. Appl. Earth Obs. Geoinf.* **2020**, *92*, 102179. [CrossRef]
31. Liu, M.; Zhai, H.L.; Zhang, X.C.; Dong, X.F.; Hu, J.X.; Ma, J.Y.; Sun, W. Time-lag and accumulation responses of vegetation growth to average and extreme precipitation and temperature events in China between 2001 and 2020. *Sci. Total Environ.* **2024**, *945*, 174084. [CrossRef] [PubMed]
32. Xu, F.; Deng, X.D.; Li, H.R.; Liu, Z.J.; Wang, Z.M.; Wang, B.H.; Zhou, P.; Niu, J.Q. Vegetation Responses to Climate Extremes Across China: Lagged Effects and Dominant Drivers Revealed by Long-Term kNDVI Observations. *Atmosphere* **2026**, *17*, 227. [CrossRef]

33. Xu, X.X.; Yuan, Q.Z.; Zhao, P.; Jia, L.P.; Ren, P. Time-lag and cumulative drought effects decouple vegetation sensitivity from damage risk in the upper Yangtze River basin. *Ecol. Indic.* **2026**, *185*, 114739. [CrossRef]
34. Zhang, F.F.; Yang, W.; Sha, D.D. Temperature-driven nonlinear thresholds and time-lags in vegetation response to extreme climate events via machine learning: Evidence from China's Poyang Lake. *Ecohydrol. Hydrobiol.* **2025**, *25*, 100685. [CrossRef]
35. Jing, J.L.; Liu, G.L.; Wang, Y.F.; Zen, Y.; Zhao, T.; Ye, Y.H. Evolution of Extreme Climate and Its Impact on Vegetation NDVI in the Yangtze River Basin from 2001 to 2022. *Environ. Sci.* **2026**, *47*, 3770–3783. [CrossRef] [PubMed]
36. Wang, J.; You, J.G.; Yi, M.X.; Huo, W.Q.; Zhang, D.M.; Shen, Y.L.; Sui, K. Cumulative and lagged effects of climate factors on vegetation end of the growing season in the Yangtze River Basin. *J. Environ. Manag.* **2026**, *404*, 129412. [CrossRef] [PubMed]
37. Chen, F.Y.; Lin, A.W.; Zhu, H.J.; Niu, J.Q. Quantifying climate change and ecological responses within the Yangtze River Basin, China. *Sustainability* **2018**, *10*, 3026. [CrossRef]
38. Xu, Y.; Zheng, Z.W.; Guo, Z.D.; Dou, S.Q.; Huang, X.T. Dynamic changes in vegetation NDVI in the Yangtze River Basin from 2000 to 2020 and detection of influencing factors. *Environ. Sci.* **2022**, *43*, 3730–3740. [CrossRef] [PubMed]
39. Wu, J.; Gao, X.J. A gridded daily observation dataset over China and its comparison with other datasets. *Chin. J. Geophys.* **2013**, *56*, 1102–1111. [CrossRef]
40. Editorial Committee of the Vegetation Atlas of China, Chinese Academy of Sciences. *Vegetation Atlas of China: 1:1,000,000*; Science Press: Beijing, China, 2001.
41. Sen, P.K. Estimates of the Regression Coefficient Based on Kendall's Tau. *J. Am. Stat. Assoc.* **1968**, *63*, 1379–1389. [CrossRef]
42. Benjamini, Y.; Hochberg, Y. Controlling The False Discovery Rate—A Practical And Powerful Approach To Multiple Testing. *J. R. Stat. Soc. Ser. B Methodol.* **1995**, *57*, 289–300. [CrossRef]
43. Cortes, J.; Mahecha, M.; Reichstein, M.; Brenning, A. Accounting for multiple testing in the analysis of spatio-temporal environmental data. *Environ. Ecol. Stat.* **2020**, *27*, 293–318. [CrossRef]
44. Jiang, W.X.; Niu, Z.G.; Wang, L.C.; Yao, R.; Gui, X.; Xiang, F.F.; Ji, Y.X. Impacts of Drought and Climatic Factors on Vegetation Dynamics in the Yellow River Basin and Yangtze River Basin, China. *Remote Sens.* **2022**, *14*, 930. [CrossRef]
45. Baba, K.; Shibata, R.; Sibuya, M. Partial correlation and conditional correlation as measures of conditional independence. *Aust. N. Z. J. Stat.* **2004**, *46*, 657–664. [CrossRef]
46. Piao, S.L.; Fang, J.Y.; Zhou, L.M.; Guo, Q.; Henderson, M.; Ji, W.; Li, Y.; Tao, S. Interannual variations of monthly and seasonal normalized difference vegetation index (NDVI) in China from 1982 to 1999. *J. Geophys. Res. Atmos.* **2003**, *108*, 4401. [CrossRef]
47. Yu, C.; Li, W.X.; Liu, C.S.; Wang, Y.; He, R.M.; Wang, G.Q. Historical evolution and future trend of meteorological drought in the upper Yangtze River basin. *Clim. Dyn.* **2025**, *63*, 415. [CrossRef]
48. Niu, N.; Li, J.P. The Features of the Heavy Drought Occurring to the South of the Yangtze River in China as well as the Anomalies of Atmospheric Circulation in Autumn 2004. *Chin. J. Atmos. Sci.* **2007**, *31*, 254–264. [CrossRef]
49. Xue, Y.K.; Diallo, I.; Li, W.K.; Neelin, J.D.; Chu, P.C.; Vasic, R.; Guo, W.D.; Li, Q.; Robinson, D.A.; Zhu, Y.J.; et al. Spring Land Surface and Subsurface Temperature Anomalies and Subsequent Downstream Late Spring-Summer Droughts/Floods in North America and East Asia. *J. Geophys. Res. Atmos.* **2018**, *123*, 5001–5019. [CrossRef]
50. Chen, S.Y.; Qiu, R.N.; Chen, Y.M.; Gong, W.; Han, G. Impacts of Drought and Heatwave on the Vegetation and Ecosystem in the Yangtze River Basin in 2022. *Remote Sens.* **2024**, *16*, 2889. [CrossRef]
51. Yi, L.; Sun, Y.; Ouyang, X.; Yin, S.H. Identifying the Impacts of Climate Change and Human Activities on Vegetation Cover Changes: A Case Study of the Yangtze River Basin, China. *Int. J. Environ. Res. Public Health* **2022**, *19*, 6239. [CrossRef] [PubMed]
52. Farris, S.; Deidda, R.; Viola, F.; Mascaro, G. On the Role of Serial Correlation and Field Significance in Detecting Changes in Extreme Precipitation Frequency. *Water Resour. Res.* **2021**, *57*, e2021WR030172. [CrossRef]
53. Piao, S.L.; Liu, Q.; Chen, A.P.; Janssens, I.A.; Fu, Y.S.; Dai, J.H.; Liu, L.L.; Lian, X.; Shen, M.G.; Zhu, X. Plant phenology and global climate change: Current progresses and challenges. *Glob. Change Biol.* **2019**, *25*, 1922–1940. [CrossRef] [PubMed]
54. Piao, S.L.; Wang, X.H.; Park, T.; Chen, C.; Lian, X.; He, Y.; Bjerke, J.W.; Chen, A.P.; Ciais, P.; Tømmervik, H.; et al. Characteristics, drivers and feedbacks of global greening. *Nat. Rev. Earth Environ.* **2020**, *1*, 14–27. [CrossRef]
55. Jiang, J.; Zhou, T.J. Observational Constraint on the Contributions of Greenhouse Gas Emission and Anthropogenic Aerosol Removal to Tibetan Plateau Future Warming. *Geophys. Res. Lett.* **2023**, *50*, e2023GL105427. [CrossRef]
56. Li, P.X.; Furtado, K.; Zhou, T.J.; Chen, H.M.; Li, J. Convection-permitting modelling improves simulated precipitation over the central and eastern Tibetan Plateau. *Q. J. R. Meteorol. Soc.* **2020**, *147*, 341–362. [CrossRef]
57. Ma, Y.M.; Li, M.Y.; Yao, H.M.; Chen, P.; Pan, H.Z. Change of NDVI in the Upper Reaches of the Yangtze River and Its Influence on the Water-Sand Process in the Three Gorges Reservoir. *Sustainability* **2025**, *17*, 739. [CrossRef]

Disclaimer/Publisher's Note: The statements, opinions and data contained in all publications are solely those of the individual author(s) and contributor(s) and not of MDPI and/or the editor(s). MDPI and/or the editor(s) disclaim responsibility for any injury to people or property resulting from any ideas, methods, instructions or products referred to in the content.